MNRAS 000, 1–17 (2017) Preprint 9 March 2018 Compiled using MNRAS LaTeX style file v3.0

The Evolution of Temperature and Bolometric Luminosity in Type-II Supernovae

T. Faran,[1]⋆ E. Nakar,[2] and D. Poznanski[2]
[1] Racah Institute of Physics, The Hebrew University of Jerusalem, Jerusalem 91904, Israel
[2] School of Physics and Astronomy, Tel-Aviv University, Tel Aviv 69978, Israel.

Accepted XXX. Received YYY; in original form ZZZ

ABSTRACT

In this work we present a uniform analysis of the temperature evolution and bolometric luminosity of a sample of 29 type-II supernovae (SNe), by fitting a black body model to their multi-band photometry. Our sample includes only SNe with high quality multi-band data and relatively well sampled time coverage. Most of the SNe in our sample were detected less than a week after explosion so their light curves cover the evolution both before and after recombination starts playing a role. We use this sample to study the signature of hydrogen recombination, which is expected to appear once the observed temperature drops to $\approx 7,000$K. Theory predicts that before recombination starts affecting the light curve, both the luminosity and the temperature should drop relatively fast, following a power-law in time. Once the recombination front reaches inner parts of the outflow, it sets the observed temperature to be nearly constant, and slows the decline of the luminosity (or even leads to a re-brightening). We compare our data to analytic studies and find strong evidence for the signature of recombination. We also find that the onset of the optical plateau in a given filter, is effectively the time at which the black body peak reaches the central wavelength of the filter, as it cools, and it does not correspond to the time at which recombination starts affecting the emission.

1 INTRODUCTION

Type II supernovae (SNe) are defined by the prominent hydrogen lines in their spectra. They are believed to originate from the collapse of an iron core of massive stars ($\gtrsim 8\ M_\odot$) that retain their hydrogen envelope. The most common subtype, comprising ~ 70 percent of all type II SNe, is characterized by a phase of of a roughly constant magnitude in the optical bands, hence their name type II-Plateau (II-P). This plateau phase typically starts 1–2 weeks after the explosion and lasts for ~100 d. Pre-explosion images have revealed that the progenitors of this class are red supergiants, in the mass range of (7–16 $M_\odot$) (Smartt 2015; for individual progenitor detections see e.g. Van Dyk et al. 2003a, Van Dyk et al. 2003b, Van Dyk et al. 2012). Type II-Linear (II-L) SNe constitutes another subclass of type II SNe (e.g., Patat et al. 1994; Arcavi et al. 2012; Faran et al. 2014a,b). They are spectroscopically very similar to type II-P events (Faran et al. 2014b, see), but their light curves are declining in all bands. In both types (II-P and II-L) there is typically a sharp drop in the luminosity after ~100 d and the luminosity starts to follow roughly the exponential decay expected from emission powered by the decay of ^{56}Ni. The distinction between these two classes is not well defined, and studies have used different definitions for II-L SNe. However, several recent works have shown that there exists a continuum of decline rates between slow declining and fast declining SNe (Anderson et al. 2014; Faran et al. 2014a), which suggests that a separation into two different classes may be artificial. Other type II sub-classes will not be discussed here. In this paper we focus on the light curves of type II-P and type II-L SNe, without making the distinction between the two types, and refer to them in short as type II SNe. Our goal here is to perform a uniform analysis of the bolometric luminosity and temperature evolution of a large sample of type II SNe and to compare our findings to theoretical models, focusing on the transition to the plateau, which takes place during the first two weeks.

There are several dozen type II SNe with detailed multi-wavelength observations. These are typically presented and analyzed individually (e.g., Leonard et al. 2002b; Maguire et al. 2010; Pastorello et al. 2009; Inserra et al. 2011; Takáts et al. 2014, 2015; Fraser et al. 2011; Tomasella et al. 2013; Dall'Ora et al. 2014; Barbarino et al. 2015; Valenti et al. 2015). There are only a few studies that analyze the bolometric properties and temperatures of a sample of type-II SNe. Bersten & Hamuy (2009) extracted bolometric light curves and effective temperature evolution for 33 SNe II-P, using calibrations for bolometric corrections from 3 well observed SNe. Valenti et al. (2016) derived the effective temperature from black body fits to photometric data of 30 type-II SNe, and calculated pseudo-bolometric light curves by integration over the optical bands. Lusk (2016) provides bolometric light curves and temperatures for 5 peculiar type II-P SNe that originated from blue supergiants, by integrating over the observed photometry and correcting for the missing flux in the UV.

The theoretical interpretation of type II light curves is that the emission until the end of the plateau is dominated by the cooling emission, i.e., the leakage of radiation energy that was deposited in the envelope by the shock that unbinds it (Falk & Arnett 1977). Energy deposited by the decay of ^{56}Ni may contribute to this phase (e.g., Falk & Arnett 1977; Young 2004; Utrobin 2007), but this contribution is found to be subdominant (Nakar et al. 2016). The end of the plateau marks the release of all the internal energy deposited by the shock in the envelope. At later times the SN enters its nebular phase and the entire luminosity is driven by the decay of ^{56}Ni.

During the early stages of the light curve ($\sim 1-3$ weeks) the leakage of radiation is facilitated mostly by the drop in the optical depth of the outflow due to its expansion (Arnett 1980). Models predict that during this phase both the temperature and the bolometric luminosity drop roughly as power-laws in time (Nakar & Sari 2010; Rabinak & Waxman 2011; Shussman et al. 2016a). Once the observed temperature drop to ≈ 7000 K, hydrogen recombination becomes important and a recombination front starts moving from the outside towards inner parts of the ejecta. During this phase, recombination, rather then expansion, is the main driver of the drop in the optical depth of the outflow. As a result the observed temperature remains almost constant while the luminosity starts dropping much more slowly or even rises.

In this work we derive the temperatures and bolometric evolution of 29 type-II SNe with high quality multi-band light curves, by fitting a black body spectrum to their spectral energy distribution (SEDs). As will be discussed extensively below, these are far from trivial. SNe II are not blackbodies, and at different times several effects lead to systematic offsets from a pure black body in various bands. Nevertheless, guided by the data and theoretical insight, we derive the underlying black body properties. We compare the temporal evolution of the temperature and luminosity to theoretical predictions, paying special attention to signs of the recombination processes in the envelope. In Section 2 we describe the contents of our SN sample and the data, in Section 3 we explain how the black body fits to the data are done. Section A describes the results of the fitting and the possible effect of extinction on the results, and Section 5 presents a comparison of our results to theoretical expectations. We summarize our results in Section. 6.

2 THE SAMPLE

We construct from the literature a sample of 29 type-II SNe with good temporal coverage and multi-band photometry. The sample mostly relies on the SNe collected in Pejcha & Prieto (2015), Faran et al. (2014a) and (Faran et al. 2014b). The SNe in the sample were required to have sufficiently early data (starting less than 20 days after the explosion) and a well sampled light curves so the early behavior could be compared to the late behavior and to theoretical models. Some objects did not enter the sample despite having well sampled photometric curves, because their data was not good enough to produce good quality temperature and luminosity curves. Ten of the objects have *Swift* UV observations, 10 have JHK data, and 7 objects have both JHK and UV. The photometric data were corrected for galactic extinction according to Cardelli et al. (1989), but not for host galactic extinction, since there is no method that can provide an accurate estimate for $E(B-V)_{host}$ (see for example the discussion in Faran et al. 2014a). We note however, that Faran et al. (2014a) found that $E(B-V)_{host}$ is typically small, of order 0.1 for nearby SNe. The explosion day is set as the mid-point between the first detection and the last non-detection of the SN, and the uncertainty is conservatively set as half the difference. Distance measurements were collected from NED[1] and averaged, using only distances based on the Tully-Fisher method, Cepheids, and SNe Ia. All of the objects are at low redshift with z<0.03. The SN properties and their references are summarized in Table. 1.

3 BLACK BODY FITTING

We calculate the temperature and bolometric luminosity of the SNe at each epoch by fitting a black-body to the photometric data, according to $L_{bol} = 4\pi\sigma T^4 R^2$. We create a two-dimensional grid of temperatures evenly spaced by 20K, and black body radii (R) in the range of 10^{12}–10^{16}cm with spacing that corresponds to 0.002 mag. We then compute synthetic photometry from the black body distribution for every T and R values in each of the filter bands. Since data in different photometric bands were sometimes taken at different epochs, linear interpolation is used to account for the missing epochs. The interpolation is constrained to a maximum of 10 days from the nearest data point at early or late phases (before day 10 or after day 70), and to 20 days during intermediate phases, where the SN properties evolve more slowly.

A correct estimation of the photometric uncertainties is needed when fitting a black body to the photometry. Due to the relatively small number of data points, the fit is sensitive to errors that are under- or over-estimated. We therefore set a minimum value of 0.05 magnitudes to the error (such that the error is the maximal value between the given photometric error and 0.05 mag), which is a typical value for the scatter in our light curves. We assign the effective wavelength of the filter transmission curve to each band, and fit the data to find the black body temperature and radius by minimizing χ^2. The uncertainty on the temperature is found by marginalizing the likelihood over the radius and finding the upper and lower temperature where $\chi^2 = \chi^2_{\rm min} + 1$. To find the uncertainty in the luminosity, we calculate L_{bol} for every T and R, and find the contour in which $\chi^2 = \chi^2_{\rm min} + 1$. The maximal and minimal values of L_{bol} are taken to be the upper and lower errors, respectively.

The SN spectrum is expected to follow a black body shape only in a limited frequency range, where $h\nu \sim kT$. At high frequencies the flux is suppressed by line blanketing, and at much lower frequencies, in the Rayleigh-Jeans (RJ) regime, it is predicted to be brighter than the RJ tail due

[1] The NASA/IPAC Extragalactic Database (NED) is operated by the Jet Propulsion Laboratory, California Institute of Technology, under contract with the National Aeronautics and Space Administration (NASA).

Table 1. SN Sample Details

SN name	Bands	Explosion day (MJD)	μ	z_{host}	Reference
SN1999em	U,B,V,R,I,J,H,K	51476 ± 4	29.84 ± 0.05	0.002	Leonard et al. (2002a) Pejcha & Prieto (2015)
SN1999gi	B,V,R,I	51519 ± 4	30.24 ± 0.04	0.002	Faran et al. (2014a)
SN2000dc	B,V,R,I	51762 ± 4	32.93 ± 0.14	0.010	Faran et al. (2014a)
SN2001cm	B,V,I	52064 ± 1	33.18 ± 0.10	0.011	Faran et al. (2014a)
SN2001cy	B,V,R,I	52086 ± 6	33.01 ± 0.12	0.015	Faran et al. (2014b)
SN2001do	B,V,R,I	52134 ± 2	32.35 ± 0.15	0.010	Faran et al. (2014b)
SN2001fa	B,V,R,I	52198 ± 3	34.24 ± 3.42	0.017	Faran et al. (2014b)
SN2001x	B,V,R,I	51963 ± 5	31.59 ± 0.11	0.005	Faran et al. (2014a)
SN2002gd	B,V,R,I	52553 ± 15	32.90 ± 0.21	0.009	Faran et al. (2014a)
SN2003hf	B,V,R,I	52864 ± 2	35.51 ± 3.55	0.031	Faran et al. (2014b)
SN2003hk	B,V,R,I	52860 ± 2	34.41 ± 0.20	0.023	Faran et al. (2014b)
SN2003iq	B,V,R,I	52920 ± 2	32.28 ± 0.08	0.008	Faran et al. (2014a)
SN2003z	B,V,R,I	52665 ± 5	31.23 ± 3.12	0.004	Faran et al. (2014a)
SN2004A	B,V,R,I	53007 ± 7	31.61 ± 0.32	0.003	Gurugubelli et al. (2008) Maguire et al. (2010)
SN2004du	B,V,R,I	53228 ± 2	33.94 ± 0.13	0.017	Faran et al. (2014a)
SN2004et	U,B,V,R,I,J,H,K	53271 ± 1	28.41 ± 0.07	0.000	Maguire et al. (2010)
SN2005cs	Swift UVOT,U,B,V,R,I,J,H,K	53549 ± 0	29.36 ± 0.01	0.002	Pastorello et al. (2009)
SN2006bp	Swift UVOT,U,B,V,r,i	53834 ± 1	31.11 ± 0.05	0.004	Quimby et al. (2007)
SN2007od	Swift UVOT,U,B,V,R,I,J,H,K	54399 ± 8	32.29 ± 0.17	0.006	Inserra et al. (2011)
SN2008in	Swift UVOT,U,B,V,R,I,J,H	54822 ± 10	30.52 ± 0.09	0.005	Roy & Kumar (2012)
SN2009N	Swift UVOT,B,g,V,R,r,I,i,J,H	54845 ± 11	31.68 ± 0.08	0.003	Takáts et al. (2014)
SN2009bw	Swift UV,U,B,V,R,I,J,H,K	54917 ± 3	30.60 ± 0.02	0.004	Inserra et al. (2012)
SN2009ib	U,u,B,g,V,R,r,I,i,J,H	55041 ± 10	31.48 ± 0.31	0.004	Takáts et al. (2015)
SN2012A	Swift UVOT,U,B,g,V,R,r,I,i,J,H,K	55929 ± 5	29.72 ± 0.17	0.003	Tomasella et al. (2013)
SN2012aw	Swift UVOT,U,u,B,g,V,R,r,I,i,J,H,K	56002 ± 1	29.89 ± 0.07	0.003	Bose et al. (2013) Dall'Ora et al. (2014)
SN2012ec	u,B,g,V,R,i,J,H,K	56143 ± 10	31.57 ± 0.45	0.005	Barbarino et al. (2015)
SN2013ab	Swift UVOT,U,B,g,V,R,r,I,i	56340 ± 1	31.71 ± 0.66	0.005	Bose et al. (2015a)
SN2013by	Swift UV,u,B,g,V,r,i	56407 ± 11	30.84 ± 0.15	0.004	Valenti et al. (2015)
SN2013ej	Swift UV *,U,u,B,g,V,R,r,I,i	56497 ± 1	29.77 ± 2.98	0.002	Richmond (2014) Valenti et al. (2014)

to the fact that the thermalization depth in this range is frequency dependent (Shussman et al. 2016a). We observe both effects in our data, and fit a black body only to the wavelength regions where it provides a good approximation.

In agreement with the theoretical predictions, we see that at high temperatures JHK observations cannot be well described by a standard black body spectrum, and tend to systematically lie above the RJ tail. This effect was recently modeled analytically by Shussman et al. (2016a) and will be further discussed in section 5.3. In the cases where this discrepancy is observed, we use only UV and optical data, and exclude the JHK bands.

As the temperature drops below $\sim 10,000 - 12,000$K, line blanketing by iron group elements becomes strong and creates a deficiency in the measured UV flux, compared to a pure black body. The main species responsible for the strong absorption are Fe III and Ti III (Kasen & Woosley 2009). Line opacity is highly sensitive to the temperature, and even a slight cooling of the photosphere induces a fast recombination of Fe III and Ti III to Fe II and Ti II (Kasen & Woosley 2009; Eastman et al. 1996). The flux absorption becomes stronger and shifts further to the optical bands as the temperature continues to decrease to $8,000$K. Figure.1 demonstrates the effect of line blanketing on the SED of SN2012aw on day 41. Data taken at wavelengths shorter than 5000 were found to be affected by line blanketing and were excluded from the fit (grey points), and only bands with wavelengths longer than 5000 were used (red points). The resulting black body at a temperature of 6420K fits the red points very well and is also in very good agreement with a spectrum taken at the same epoch. The observed spectrum also confirms the flux cut-off around the *B*-band. In order to determine the time where the flux in each photometric band is suppressed by line-blanketing, we run the black body fitting procedure on each of the following filter groups: UV-UBVRIJHK, UBVRIJHK, BVRIJHK, VRIJHK and RIJHK, i.e., each time excluding the bluest band. We first determine, as an example, when the flux in the UV bands falls below the black body curve by looking at the fit to the UBVRIJHK regime. As long as the temperature is high enough, the UV flux will appear above the black body fit to UBVRIJHK or right on it. However, as the temperature decreases enough such that line blanketing starts to have an effect on the UV flux, the UV data points will drop below the UBVRIJHK curve. We exclude a certain band from the fit when it is 1-σ below the black body curve. This means that until that epoch we can use the UV-UBVRIJHK bands to determine the black body parameters, and from that day on we can only use the UBVRIJHK bands to fit the data. This procedure is repeated with the other bands to determine when the U, B, and V bands are affected by line blanketing and need to be excluded. The transition days coincide with the intersection between the temperature curves calculated with the bluest band, and the one calculated without it. Eventually, we construct the final temperature and luminosity curves using the transitions determined for each of the objects.

At early phases, when the temperature is higher than 10^4K, the peak of F_λ occurs at wavelengths shorter than 3000 and UV observations are therefore crucial to constrain the fit parameters. JHK observations lie far from the peak of F_λ even at low temperatures (~6000 K), and therefore do not play a critical role in constraining the temperature. However, due to the exclusion of many of the bluer bands by line blanketing, it is necessary to have more data points in the red to improve the fit, meaning that JHK data become important at late epochs.

In order to quantify the importance of UV and Infra-Red (IR) photometry, we run a simulation and estimate the expected errors on the temperature in the absence of UV and IR. We produce synthetic photometry from black body distributions at temperatures 5000K–25,000K in 1000K bins, simulating a spread in the data using the typical photometric errors in each band. We then fit the synthetic data to a black body, repeating the process 100 times per temperature bin. The mean value and standard deviation (STD) of the best-fitting temperatures are computed, where we treat the STD as a measure of the typical statistical error. The uncertainties deduced from the simulation are presented as a function of the temperature in Figure. 2. From the upper panel of Figure. 2 one can see that at temperatures of ~20,000K, the uncertainties on the temperature are quite high (over 800K) even with UV data. This reflects the fact that F_λ peaks at ~1300, while the effective wavelength of the bluest filter we use ($Swift-uvw2$) is only at 2230. Below T=15,000K, fits that do not include UV (but do include U) are able to reproduce the temperature with an accuracy of ~500K. When U-band data is excluded, the fit reaches that accuracy below T=12,000K.

At lower temperatures, corresponding to late epochs, most of the flux at wavelengths shorter than the B band is already affected by line blanketing and only bands with effective wavelengths longer than the V band can be used. In the bottom panel of Figure 2 it is evident that JHK data are important at T>7000K if the B band is not included, as the STD of the fit temperature is relatively high and rises rapidly with the model temperature. Although fitting with the V, R and I bands is still able to produce errors below 10%, we will see in Section 4.1 that the flux in the V band is typically absorbed by iron blanketing at ~6000K. In the absence of JHK observations, we are left with only 3 data points for many objects - V, R and I. In these cases, it is impossible to determine when the V band falls below the black body curve, since we cannot examine the fit done without V, having only 2 data points at longer wavelengths. As a result, when an object does not have JHK data we typically cannot trust the temperature curve below ~6000K and we do not fit the data below this temperature.

Throughout this paper, we consider only objects with U or UV data to deduce physical parameters at high temperatures (above ~10,000K), and objects with JHK data at low temperatures (below ~6000K).

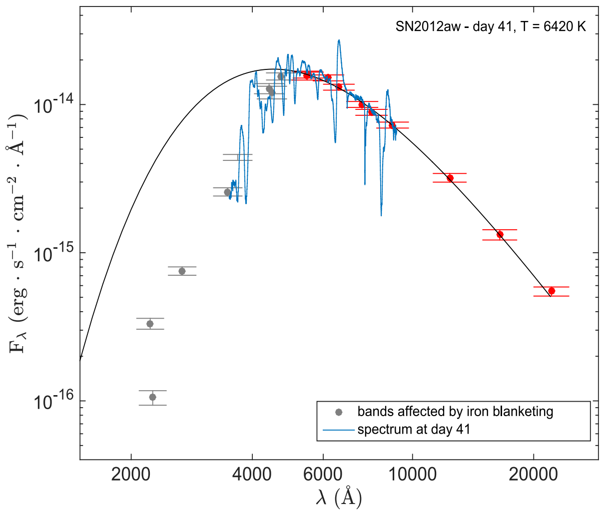

Figure 1. Black body fit of SN2012aw on day 41. The grey points represent bands that are affected by iron-blanketing and were therefore excluded from the fit. The black body curve fits the data very well above 5000, whereas at shorter wavelengths the SED is no longer represented by a black body. A spectrum taken on day 41 (Bose et al. 2013) is also shown to coincide well with the data, and confirms the flux cutoff around the $\boldsymbol{B}$-band.

4 RESULTS

4.1 Temperature

The temperature curves are computed from the black body fits at each epoch and are presented in Figure. 3 (a list of all the results is also available in Appendix. A). After the explosion, the envelope expands and cools adiabatically. The typical temperatures during the first 10 days are above 10,000 degrees. In cases where UV data exist, the typical errors for that temperature range are smaller than ~500K, and are comparable to the errors predicted by our simulations (see Section 3). Between 20 and 40 days after the explosion, the temperature curves start evolving more slowly compared to early phases. The flattening typically happens between 6000K and 7000K, and is therefore consistent with being associated with a recombination wave that propagates into the envelope and dictates the black body temperature to be the temperature of hydrogen recombination. This effect is analyzed and discussed in Section 5.2. We note that objects without JHK data do not show this flattening, since as discussed in Section 3, for these SNe we were not able to determine the time where the V-band can no longer be used and the fit stops when the temperature reaches 6000K.

As in Valenti et al. (2016), we observe that excluding UV data from the fit systematically leads to lower temperatures. This is true also for U, B and V, where the temperature produced without the bluest band is lower than that produced with it, before its flux is affected by iron blanketing. Since we do not observe this behavior in the simulation described in Section 3, the effect is not statistical and points to a deviation of the spectrum from a black body. We suggest that this is related to the re-distribution of energy that is absorbed by line blanketing. Most of the absorbed

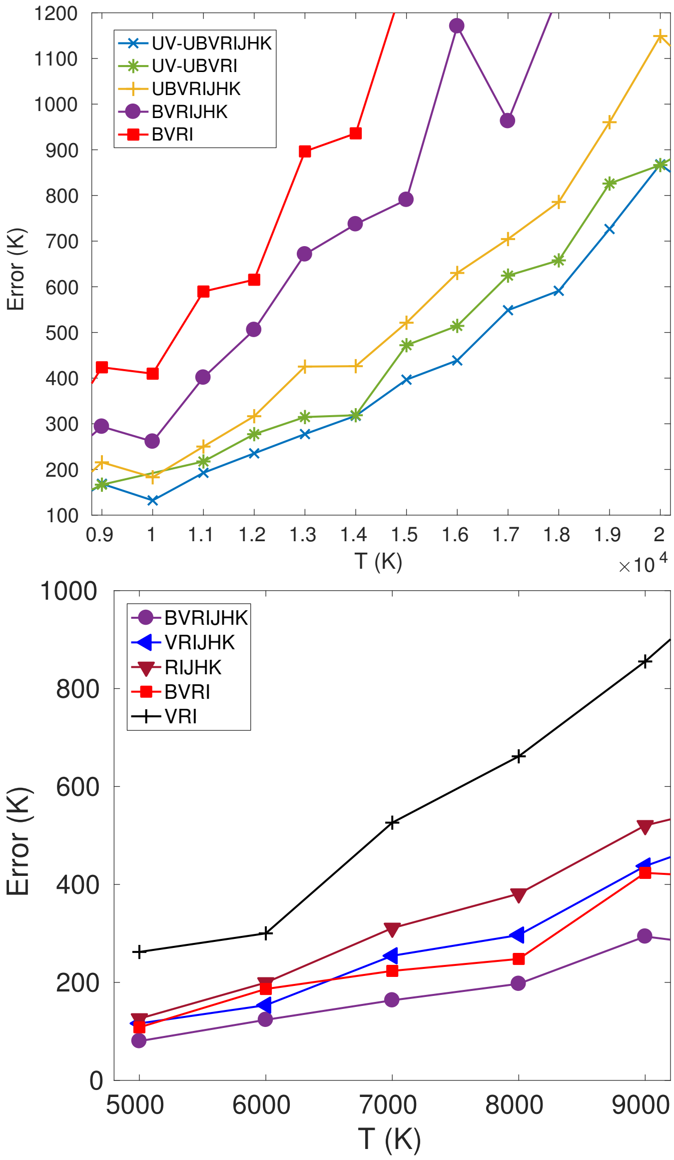

Figure 2. The expected uncertainties of the temperature of a black body, resulting from a simulation of synthetic data. The estimated uncertainties decrease as a function of the proximity of the bands to the black body peak, and therefore rise with the temperature.

radiation is expected to be re-emitted close to the absorption wavelength (see Pinto & Eastman 2000). As a result, the flux of the bluest band we use will be higher than the black body at the same temperature. Since the bands near the peak of the spectrum have the highest effect on the fit, that will result in higher fit temperatures. We redo the fits without the bluest band, and measure the flux under the resulting black body curve. We then measure the flux excess in the bands that lie above the black body curve, and the flux deficiency (due to line blanketing) in the bands below the black body curve and find that they are of the same order. This reinforces the assumption that the absorbed radiation by iron group elements is emitted at wavelengths close to the black body peak, and may add an uncertainty to the temperature and bolometric luminsoity that we measure. Above 10,000K, the temperatures calculated with the bluest band are $\approx 10\%$ higher than the ones calculated when it is omitted, and the difference becomes less significant at lower temperatures. The effect on the luminosity is higher and can get up to $\approx 10-20\%$. Therefore, the temperatures and bolometric luminosities presented in this paper can be overestimated by up to $\approx 10-20\%$.

We record the temperatures at which the flux in different bands starts being affected by line blanketing, and find that the typical temperature for UV is ~11,000K, and ~8000K in the *U* and *B* bands. The *V* band seems to be affected around ~6000K. These results agree with the temperatures shown in Eastman et al. (1996)'s Figure. 7.

Bersten & Hamuy (2009) fit a black body to the photometry of SN1999em corrected to $A_V^{host} = 0.18$ and present its temperature and bolometric luminosity curves. After correcting our data to $A_V^{host} = 0.18$, we extract the temperature curve and compare it to the middle panel in Bersten & Hamuy (2009)'s Figure. 8. We find a good agreement between the values of the temperature and its evolution. The temperature computed at the first epoch, ~ 5 days, is around 13,000K in both curves and decreases to show a "bump" around day 16. Eventually, both curves settle on a temperature of ~ 6000K in the middle of the plateau. Valenti et al. (2016) also fit a black body to several SNe that are included in our sample, but unfortunately the values are not provided, and we cannot perform a quantitative comparison.

4.2 Luminosity

The bolometric luminosity for each of the SNe is computed from the fit and the curves are presented in Figure. 4. Similarly to the temperature, the luminosity typically decreases as a power law during early epochs. The luminosity in most of the objects relents from its fast decline and starts to decrease more moderately, where the flattening seems to coincide with the break in the temperature. There are 3 objects whose luminosity not only flattens but also starts to rise. This happens for SN2004A and SN2009N at day 30 after explosion, and for SN2005cs at day 23. The transition in luminosity happens quite sharply and occurs when the temperatures are 6000K, 5900K and 6900K for the 3 objects, respectively. The change in the evolution of the luminosity is probably also related to the recombination of the envelope. We will discuss this further in Section 5. At the end of the plateau, the bolometric luminosity falls sharply.

We compare our bolometric luminosity curves to pseudo-bolometric curves from the literature by correcting for the different assumed distances to the SNe, and shifting in time to match the assumed explosion day. While broadly speaking there is mostly agreement between our work and previous efforts, there are still some discrepancies. The comparison is presented in Figure. 5. Pseudo-bolometric luminosities that were not computed with UV nor JHK data, as done for SN2009bw, SN2008in, and SN2004A, can be underestimated by up to 30%.

4.3 The Effect of Extinction

Host interstellar or circumstellar dust can introduce extinction that is not corrected for in our data (see Section 2),

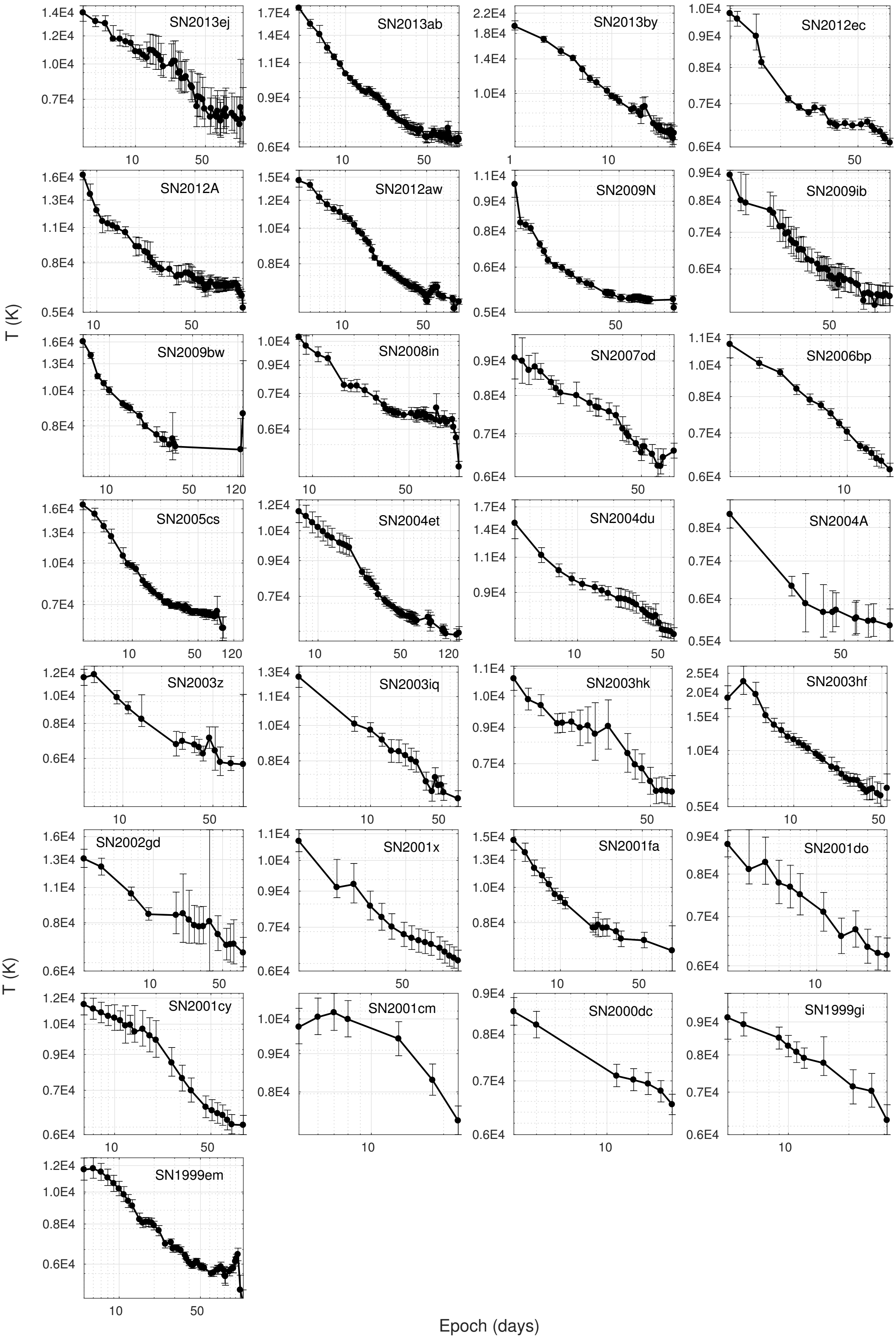

Figure 3. The temperature as a function of time for each SN in the sample.

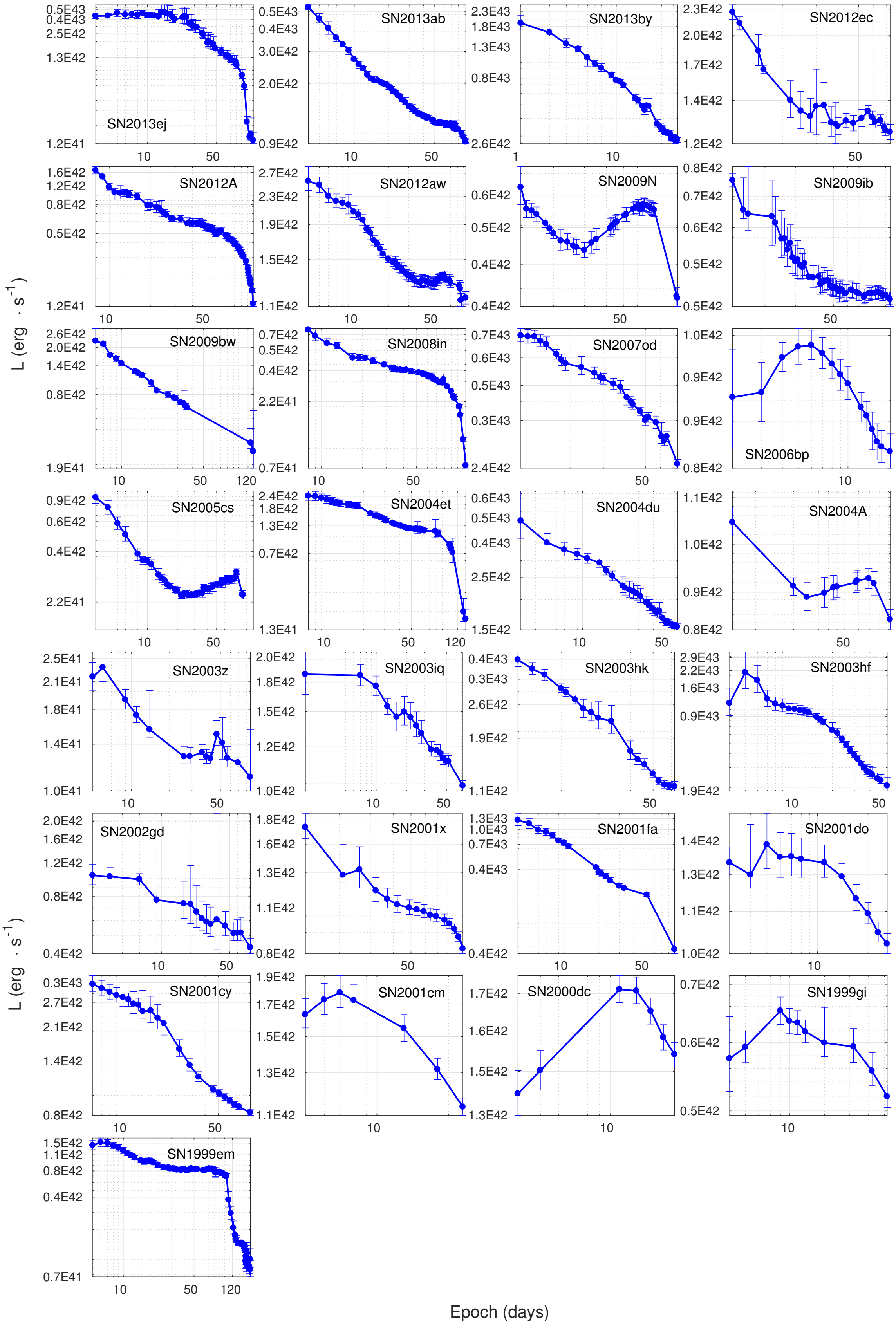

Figure 4. The bolometric luminosity curves as calculated from the black body fits for each SN in the sample.

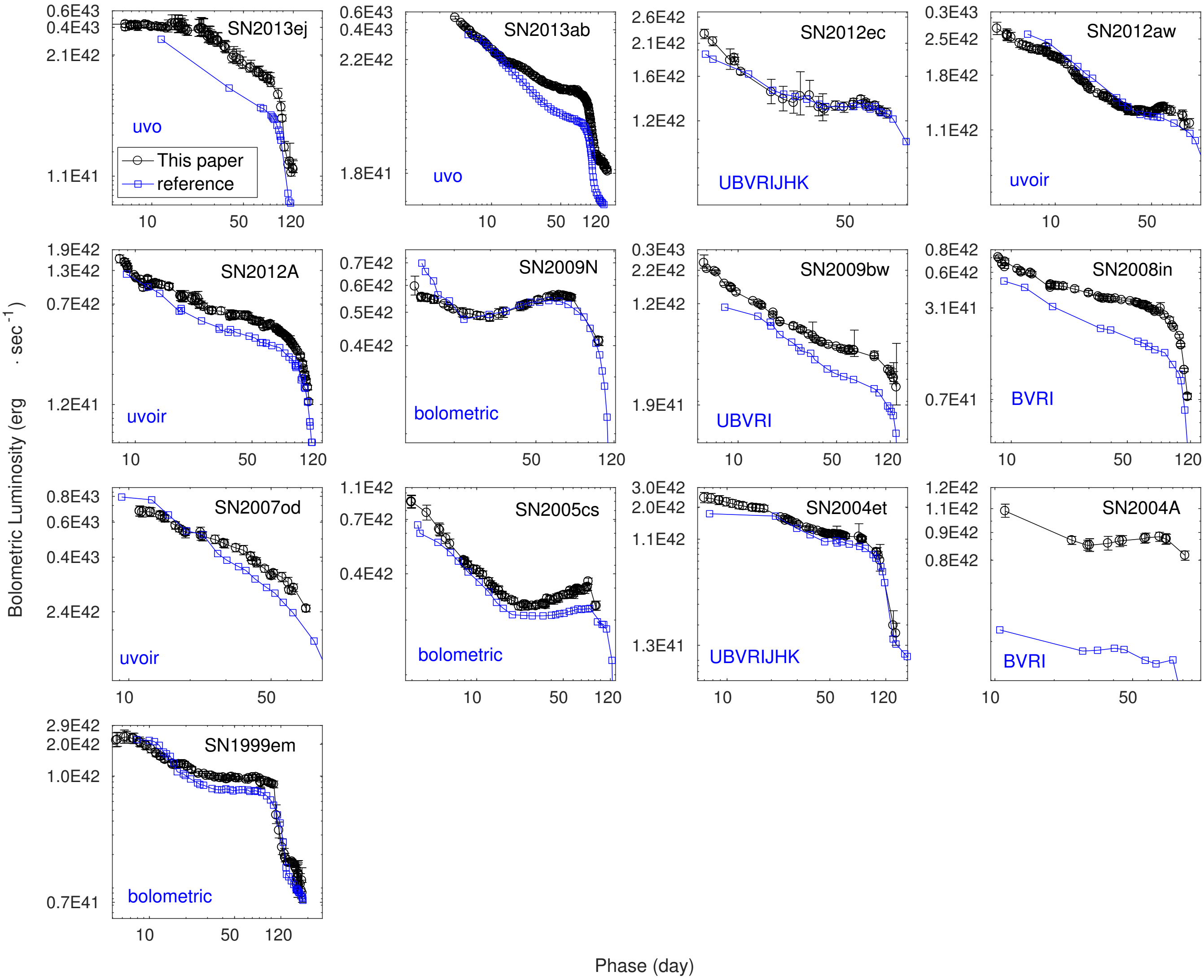

Figure 5. Comparison between the bolometric luminosity curves calculated in this paper (blue) and pseudo-bolometric curves from the literature (red), where the integrated wavelength range is specified. ***'bolometric'*** light curves include bolometric corrections or are based on black body fits. Otherwise, the light curves are the integrated luminosity in the observed bands without any bolometric corrections. The luminosity of SN1999em presented here was calculated after correcting for $A_V^{host} = 0.18$, in order to compare to Bersten & Hamuy (2009). Discrepancies between the curves at early times are probably due to missing UV flux in the pseudo-bolometic curves. SN2012ec (Barbarino et al. 2015), SN2012aw (Dall'Ora et al. 2014), SN2012A (Tomasella et al. 2013), SN2013ab (Bose et al. 2015a), SN2009N (flux in RJ was approximated by RJ tail, no corrections in the blue) (Takáts et al. 2014), SN2009bw (Inserra et al. 2012), SN2008in (Roy & Kumar 2012), SN2005cs (bolometric corrections) (Pastorello et al. 2009), SN2004et (Maguire et al. 2010), SN2004A (Hendry et al. 2006; Maguire et al. 2010), SN1999em (Bersten & Hamuy 2009), SN2007od (Inserra et al. 2011), SN2013ej (Bose et al. 2015b)

resulting in an underestimation of the fit temperatures and luminosities. Although it is quite difficult to find a good estimation for A_V^{host}, it is possible to quantify the effect a certain Av value has on the fit parameters as a function of the temperature. We repeat the fitting procedure two more times assuming E(B-V) = 0.1 and 0.05, and R_V=3.1, using the galactic extinction laws of Cardelli et al. (1989). As most type-II SNe in or sample are expected to have $E(B-V)^{host} < 0.1$ (Faran et al. 2014a), this value is effectively an upper limit on the possible required corrections.

In Figure 6 we present the relation between the best fit temperatures resulting from the correction to $E(B-V)^{host} = 0.1$ ($A_V^{host} \approx 0.3$) and $E(B-V)^{host} = 0.05$ ($A_V^{host} \approx 0.1$) as a function of the uncorrected SN temperatures. The dependence of the corrected temperatures on $T(A_V^{host} = 0)$ can be well described by a third order polynomial, according to the following relations:

$$T(A_V = 0.3) \approx 3.1T_3^3 - 58T_3^2 + 1630T_3 - 1730 \quad (1)$$

and:

$$T(A_V = 0.15) \approx 0.69T_3^3 - 9.14 \times 10^{-2}T_3^2 + 1150T_3 - 424, \quad (2)$$

where $T_3 \equiv T(Av = 0)/10^3$. These relations offer a convenient way to estimate the error on a fit temperature, in the typical extinction range of $A_V^{host} = 0 - 0.3$ mag.

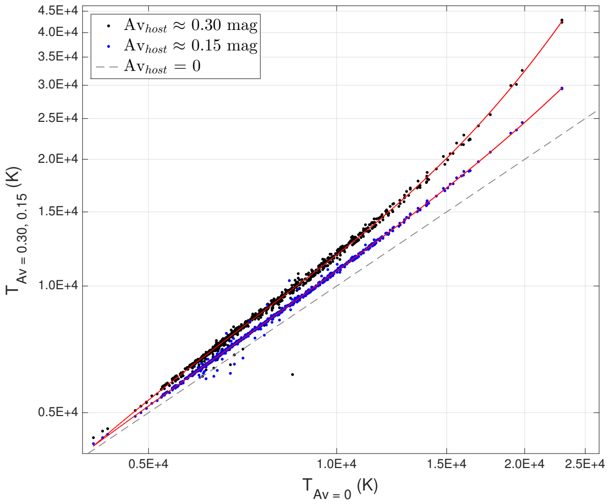

Figure 6. The best fit temperatures resuting from an extinction correction of $A_V^{host} = 0.3$ (black dots) and $A_V^{host} = 0.15$ (blue dots), as a function of $T(A_V^{host} = 0)$. The grey dashed line indicates $T = T_{A_V^{host}=0}$. The third order polynomial fits to the data are plotted in red and can be used to translate between the uncorrected and corrected temperatures.

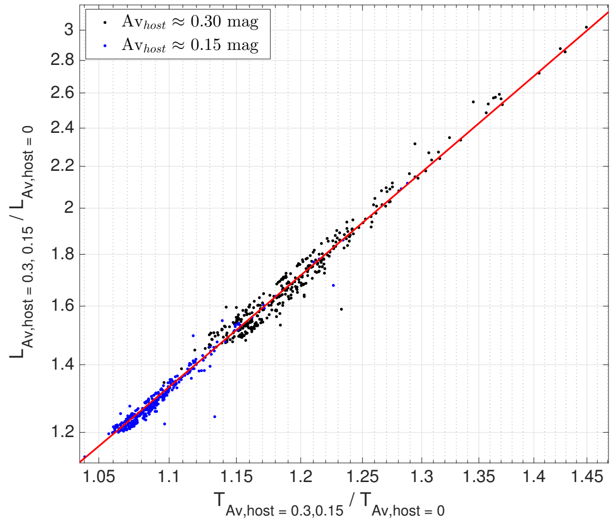

Figure 7. The ratio between the extinction corrected L_{bol} ($A_V^{host} = 0.3$ in black and $A_V^{host} = 0.15$ in blue) and the uncorrected L_{bol}, as a function of the similar temperature ratio for $T_{A_V^{host}=0} > 8000$K. Since extinction has a minimal effect on long wavelength observations, the Rayleigh-Jeans part of the spectrum at high temperatures is expected to be approximately fixed. Therefore, the data follow the relation: $\frac{L_{A_V}}{L_0} = \left(\frac{T_{A_V}}{T_0}\right)^3$, which is presented by the red line.

Since the effect of extinction on the RJ is weak, we expect the luminosity to behave as $\frac{L_{A_V}}{L_0} = \left(\frac{T_{A_V}}{T_0}\right)^3$ at high temperatures. We fit the data with $T(A_V = 0) > 8000$K according to this relation for both Av=0.3 and Av=0.15 and present the data and the fit in Figure. 7. This, together with the previous relation for the temperatures, allows also the bolometric luminosity to be corrected for extinction as the relation holds down to low temperatures of $\sim 8000K$. Below that temperature, the corrections to L are less than 10%, which is of the order of the uncertainty.

5 COMPARISON TO THEORY

5.1 The Temperature at the Beginning of the Plateau

The formation process of the plateau in Type-II SNe and the origin of its shape (i.e., its luminosity and temperature evolution) are not fully understood. The common wisdom states that the plateau is formed due to a recombination wave that propagates into the envelope in Lagrangian coordinates. The recombination front defines the photosphere and therefore also fixes its temperature to the temperature of hydrogen recombination in the envelope. According to this view, the plateau should start when T≈7500K. However, more detailed theoretical models show that the peak in each photometric band is observed slightly before the black body peak enters the observed band. This is why redder bands peak at later time. Recombination prevents the observed temperature from falling below ~6000K, which is the main reason that after the peak the luminosity in the optical and IR bands falls rather slowly, and creates what is referred to as the plateau. We therefore expect to find photospheric temperatures higher than 7500K when the plateau starts.

We define the plateau starting time, t_p, in a specific band to be the day at which the light curve changes by less than 0.02 magnitudes per day. To find t_p, we fit a low order polynomial to the first 15-20 days and find the day where the derivative equals 0.02 mag/day. In order to estimate the uncertainties in t_p, we use the photometric errors of the data to generate random Gaussians errors, from which we create simulated data. We run the fit 1000 times on simulated data and use the mean of the results as the value of t_p and the standard deviation as its uncertainty. The value of t_p can be sensitive to the order of the polynomial and to the time range chosen for the fit. The maximal discrepancies introduced by changing those parameters are typically not larger than one day. We therefore set a minimal error of one day on t_p.

In Table 2 we present the t_p values computed in the R and I bands. Some objects have only an upper limit on t_p, since they were first observed already on the plateau. Nevertheless, for most of the objects it is clear that the plateau in R starts slightly before the plateau in I, as predicted by theory. In Figure 8 we demonstrate the different locations of the plateau in the R and in the I band for SN2012aw.

The temperatures associated with t_p in R and I are computed by interpolating the temperature curves to t_p. We plot the temperatures at t_p, i.e. $T_p = T(t = t_p)$ in the R-band for each SN in Figure. 9. The blue arrows indicate the effect that $A_V^{host} = 0.3$ would have on T_p at $T \approx 8000$K and $T \approx 11,000$K, according to equation 1. Objects with only lower limits (i.e., first data point lies already on the plateau) are presented by red triangles. Almost all T_p values lie above 8000K, and many of them above 10,000K. The low luminosity SN2005cs shows an exceptionally high lower limit of $T_p \gtrsim 16,500$K. The observed range of T_p (with the exception of SN2005cs) is consistent with the theoretical light curves prediction by Shussman et al. (2016a). For example, the predicted R-band T_p for explosion energy of 10^{51} erg of progenitors with radii

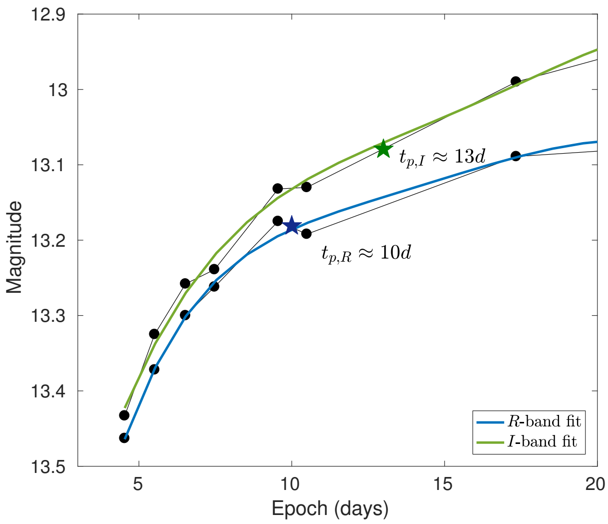

Figure 8. The locations of $t_{p,R}$ and $t_{p,I}$ of SN2012aw, as defined by the derivative of the polynomial fit to the ***R***-band (blue) and the ***I***-band (green). The plateau in the ***I***-band appears to start slightly later than the plateau in the ***R***-band.

in the range of $400-800\ R_{\odot}$ and ejecta masses in the range of $7-15\ M_{\odot}$ is between about 10,000K and 12,000K.

5.2 Signs of Recombination in the Temperature and Luminosity Curves

As discussed in Sections 4.1 and 4.2, the evolution of the temperature and the bolometric luminosity is characterized well by a power-law, that flattens when the temperature drops to ~6000–7000K. We compute the early values of the logarithmic derivatives of the luminosity and temperature, $\alpha_{\rm L}$ and $\alpha_{\rm T}$, respectively, during the first 15 days after the explosion. SNe that do not have U or UV data are excluded, since the temperatures at these epochs are typically higher than 12,000K, where U-band data (or bluer) are important to constrain the fit (see Section 3). We also calculate the late logarithmic derivatives between 40 and 100 days, while the SN light curve is on the plateau. For this we choose only SNe with IR data for the reasons discussed in Section 3. The results are summarized in Table 3. The best fit values for the early power law are highly sensitive to the exact value of the zero point in time. Since we make conservative explosion day estimates (see Section. 2), some of the uncertainties on the explosion day are as large as 5-10 days, and introduce non-negligible uncertainties to the values of the power law. The uncertainty values introduced from the fit itself and from the uncertainty on the explosion day are presented separately in Table 3. The values in the parentheses are the errors produced by the fit, and the upper and lower values are the differences from the α values that we get using the lower and upper boundaries of the explosion day estimate, respectively. In cases where the explosion day uncertainty is large (as in SN2013by, SN2012ec, SN2009jb and SN2008in) the upper and lower uncertainties are quite large. However, the explosion day uncertainty naturally has very little effect on the late values of α.

An example of the fit for α_T is shown in Figure. 10. It depicts the temperature curve of SN2005cs, on a logarithmic sacale. The best-fit logarithmic derivative computed during the first 15 days is $\alpha_{\rm T} = -0.47 \pm 0.03$, and during days 40-100 is $\alpha_{\rm T} = -0.06 \pm 0.07$. There is a clear flattening of the temperature curve between t=19d and t=35d, when the temperature is between 6500K and 7500K. In Figure 11 we present the temperature curves and the power law fits for all the objects that have both UV and IR data. From the values of the logarithmic derivatives (table 3) it is clear that at some point the temperature evolution flattens. At early time most values are in the range $\alpha_{\rm T,early}$ ~-0.6 – -0.2 while at late time all best fit values are in the range $\alpha_{\rm T,late}$ ~-0.15 – 0. The weighted mean values of the logarithmic derivatives are $\bar{\alpha}_{\rm T,early} = -0.38 \pm 0.01$ and $\bar{\alpha}_{\rm T,late} = -0.08 \pm 0.02$. Although it is not possible to point out the exact temperature of the transition, one can see that the range of temperatures between the two power law regimes is ~6000-7000K, which is the temperature range expected from hydrogen recombination in type-II SN envelopes.

We also calculate the early and late logarithmic derivatives of $L_{\rm bol}$. Similar to the temperature, the bolometric luminosity curves generally have a higher logarithmic derivative in the early phases. Most of the values of $\alpha_{\rm L,early}$ are between -0.2 and -0.8, while most values of $\alpha_{\rm L,late}$ are between -0.6 and 0.2, with weighted mean values of $\bar{\alpha}_{\rm L,early} = -0.46 \pm 0.01$ and $\bar{\alpha}_{\rm L,late} = -0.22 \pm 0.03$. When including the effect of extinction, we find that the values of $\alpha_{\rm T,early}$ and $\alpha_{\rm L,early}$ increase by ~ 0.1 and ~ 0.2 respectively, with an extinction value of $E(B-V) = 0.1$mag. This result is also consistent with the expectation from recombination which is expected to cause a flatter, or even rising, light curves once the recombination front reaches facilitate the release of radiation from inner regions.

An interesting question is whether there are correlations between the early and late evolution, or between temperature and luminosity evolution. In Figure 12 we plot $\alpha_{\rm T,late}$ vs. $\alpha_{\rm T,early}$ (upper panel) and $\alpha_{\rm L,late}$ vs. $\alpha_{\rm L,early}$ (lower panel). The color coding refers to the decline rate of the *V*-band light curve per 100 days, calculated by linearly fitting the magnitude decline rate between day 25 and 75. The figures show no clear correlations between early and late evolution or between the late decline rate and the temperature evolution (early or late). However, there is a linear correlation between $\alpha_{\rm T}$ and $\alpha_{\rm L}$.

Shussman et al. (2016a) provides theoretical predictions of $\alpha_{\rm T,early}$ and $\alpha_{\rm L,early}$ based on numerical simulations of SN explosions of a large set of RSG progenitors. They find that before recombination $\alpha_{\rm T}$ is not strictly constant, and that it makes a transition from about -0.35 to -0.6. The time of steepening in $\alpha_{\rm T}$ depends on the progenitor radius and ejecta velocity and for typical parameters it ranges between a day and two weeks. Since the data we have is not detailed enough to see the transition between the two power-laws, but only a single average power-law index, the analytic prediction is $\alpha_{\rm T,early} \approx$ -0.35 – -0.6. This range is marked in figure 12 and it is broadly consistent with the observed values listed in table 2. The theoretical model for the luminosity evolution predicts $\alpha_{\rm L,early} \approx -0.35$. This value depends slightly on the progenitor radius (up to about ±0.05) and more strongly on the progenitor structure (i.e., density profile). comparison of this prediction to the values listed in table 2 shows that they are consistent for most SNe but not for all. Moreover, the value of $\alpha_{\rm L,early}$ is inconsistent with being similar to all

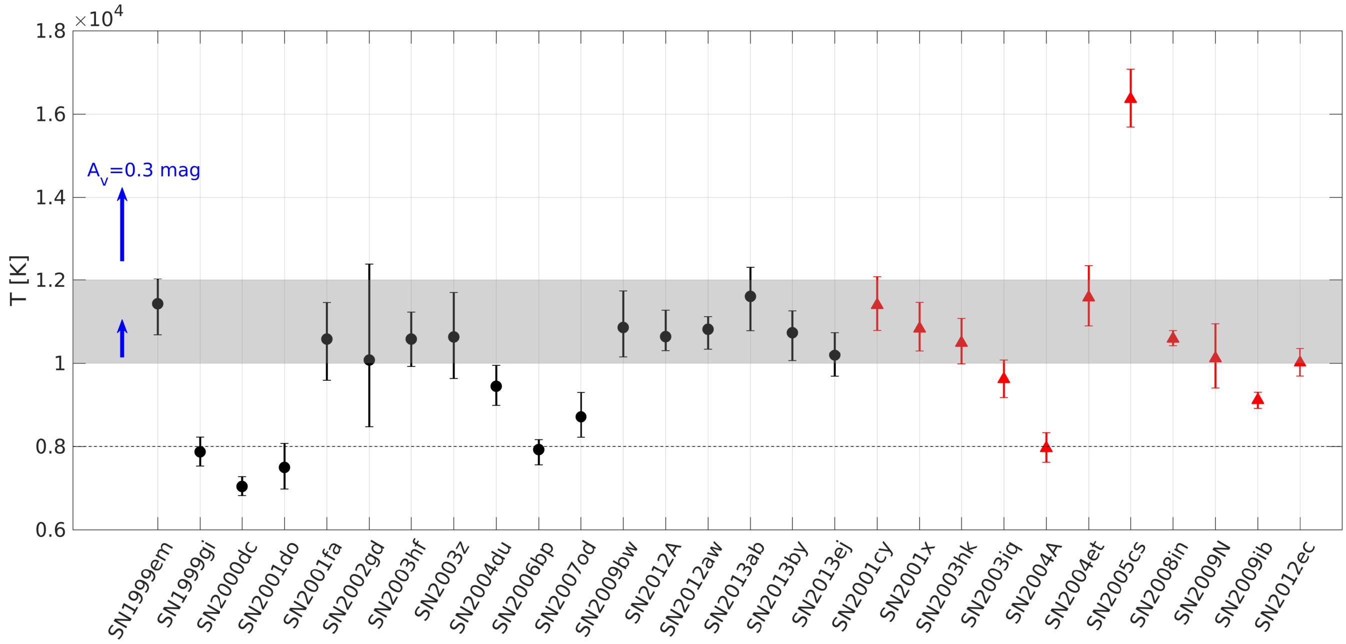

Figure 9. The temperatures at the onset of the plateau phase in the *R* band. Lower limits are marked by red triangles. The onset of the plateau is defined as the day in which the light curve changes by less than 0.02 magnitudes per day. Most of the temperatures lie above 8000K, which reinforced our claim that the flattening of the light curve is not caused by recombination. The blue arrows show the effect of extinction on T_p at T≈11000K and T≈8000K for A_V=0.3. The plateau temperatures agree with radiative transfer results calculated by Shussman et al. (2016b) for a set of 124 RSGs, represented by the shaded area.

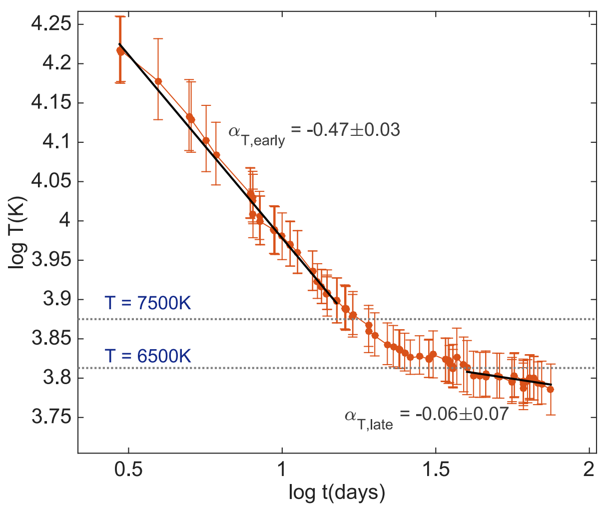

Figure 10. The temperature curve of SN2005cs on logarithmic scale. The temperature behaves as a broken power law, where in early phases it declines rapidly with a power of -0.47 ± 0.03, and at late phases the power law is -0.06 ± 0.07. This transition in the power law happens within the temperature range 6500–7500K, and we interpret it as the time when the color shell reaches the recombination temperature.

SNe. This is probably due to different density profiles of the progenitors.

5.3 Deviation from Black Body

At high temperatures, we find that a black body is not able to describe the whole observed spectrum not only at short wavelengths, where line blanketing is important, but also at long wavelengths on the RJ tail. In the left panel of Figure. 13 we show the SED of SN2012A on day 8, where the temperature is ~15,000K. The dashed blue line is the best fit to all of the data points, which clearly fails to fit the JHK observations. This effect is observed in all SNe that have early JHK data, which always seem to be brighter than the RJ tail at the temperature corresponding to the optical and UV flux.

Deviation of the RJ tail from a black body spectrum of early type II emission was seen in numerical simulations (e.g., Tominaga et al. 2011) and was modeled recently analytically by Shussman et al. (2016a). According to the model the reason for the deviation is that the flux at different wavelengths is determined at different locations in the outflow at different gas temperatures. Shussman et al. (2016a) find that on the RJ tail the modified spectrum can be approximated as $F_\nu \propto \nu^{1.4}$ and they also provide an approximation for the entire spectrum. The black solid line in the left panel of Figure. 13 is the best fit of Shussman et al. (2016a) model to the data of SN2012A. The model seems to fit the data very well throughout the UV and the IR and follows the JHK flux where it departs from a standard black body.

At lower temperatures both the standard black body model and the modified black body models are able to describe the JHK observations, as seen in the right panel of Figure. 13. The reason is that these bands are closer to the peak of the spectrum, where the models are essentially

SN name	t_p *R*-Band	T_p *R*-band	t_p *I*-Band	T_p *I*-band
SN1999em	8.0 (1.0)	11400^{+600}_{-800}	8.0 (1.1)	11400^{+700}_{-800}
SN1999gi	10.0 (1.0)	7900^{+400}_{-400}	10.0 (1.0)	7900^{+400}_{-400}
SN2000dc	13.0 (1.0)	7000^{+300}_{-300}	13.0 (1.0)	7000^{+300}_{-300}
SN2001cm			6.0*	9600^{+500}_{-500}*
SN2001cy	6.0*	11400^{+700}_{-700}*	6.0*	11400^{+700}_{-700}*
SN2001do	8.0 (1.0)	7500^{+600}_{-600}	11.0 (1.0)	7100^{+600}_{-500}
SN2001fa	8.0 (1.0)	10600^{+900}_{-1000}	9.0 (1.0)	10000^{+1000}_{-700}
SN2001x	13.0*	10800^{+700}_{-600}*	13.0*	10800^{+700}_{-600}*
SN2002gd	6.0 (3.0)	10000^{+2400}_{-1700}	6.0 (3.0)	10000^{+2400}_{-1700}
SN2003hf	13.0 (1.0)	10600^{+700}_{-700}	14.0 (1.1)	10400^{+700}_{-700}
SN2003hk	15.0*	10500^{+600}_{-600}*	16.0*	10500^{+600}_{-600}*
SN2003iq	7.0*	9600^{+500}_{-500}*	7.0*	9600^{+500}_{-500}*
SN2003z	9.0 (1.5)	11000^{+1100}_{-1100}	12.0 (1.6)	9300^{+700}_{-800}
SN2004A	11.0*	8000^{+400}_{-400}*	11.0*	8000^{+400}_{-400}*
SN2004du	10.0 (1.0)	9500^{+500}_{-500}	11.0 (1.0)	9300^{+500}_{-500}
SN2004et	9.0*	11600^{+800}_{-700}*	9.0*	11600^{+800}_{-700}*
SN2005cs	3.0*	16400^{+800}_{-700}*	3.0*	16400^{+800}_{-700}*
SN2006bp	8.0 (1.0)	7900^{+300}_{-400}	8.0 (1.0)	7900^{+300}_{-400}
SN2007od	9.0 (1.0)	8700^{+600}_{-600}	9.0 (1.0)	8700^{+600}_{-600}
SN2008in	9.0*	10600^{+200}_{-200}*	9.0*	10600^{+200}_{-200}*
SN2009N	14.0*	10100^{+900}_{-800}*	14.0*	10100^{+900}_{-800}*
SN2009bw	9.0 (1.0)	10900^{+900}_{-800}	11.0 (1.0)	9800^{+600}_{-600}
SN2009ib	13.0*	9100^{+200}_{-300}*	13.0*	9100^{+200}_{-300}*
SN2012A	13.0 (1.7)	10600^{+700}_{-400}	14.0 (1.0)	10400^{+600}_{-500}
SN2012aw	10.0 (1.1)	10800^{+300}_{-500}	13.0 (3.1)	10000^{+900}_{-1200}
SN2012ec	15.0*	10000^{+400}_{-400}*	15.0 *	10000^{+400}_{-400}*
SN2013ab	9.0 (1.0)	11600^{+800}_{-900}	9.0 (1.0)	11600^{+800}_{-900}
SN2013by	8.0 (1.0)	10700^{+600}_{-700}	8.0 (1.0)	10700^{+600}_{-700}
SN2013ej	12.0 (1.6)	10200^{+600}_{-600}	11.0 (1.4)	10400^{+600}_{-600}

Table 2. The times at which the *R*- and the *I*-bands enter the plateau phase, and the corresponding temperatures at those epochs.

equivalent. Also, at lower temperatures, where recombination starts affecting the spectrum the analytic model is no longer applicable.

6 SUMMARY

We calculated the temperaures and bolometric luminosities of 29 type-II SNe, by fitting black body models to their SEDs. We use the results to study the properties at the beginning of the plateau, to look for the signature of hydrogen recombination and to compare the observation before recombination becomes important to theoretical models. Our main findings are listed below.

• The temperature at the onset of the plateau phase in the *R*-band is above 8000K for all SNe in our sample, and exceeds 10,000K in many of them. This temperature changes as a function of the observed band, and is determined by the temperature at which the peak of the black body spectrum roughly coincides with the center of the filter transmission curve. This result is consistent with recent theoretical models and is different than the common statment that the plateau phase starts once hydrogen recombinations becomes important. The temperatures we find agree with the predicted values for typical RSG progenitors of type-II SNe (Shussman et al. 2016a).

• We find that the temperature evolves with time as a power law, which flattens at $\sim 6000-8000$K. We observe a similar evolution in the bolometric luminosity, where the logarithmic derivative at early phases is higher than that at late phases. The flattening is most likely a result of the recombination wave that exposes the inner layers. The values of the logarithmic derivatives for T and L_{bol} at early phases agree with predictions from simulations and analytic works (Shussman et al. 2016a; Nakar & Sari 2010).

• SN spectra deviate from a standard black body, both at low temperatures and short wavelengths due to line blanketing, and also at high temperatures and long wavelengths. We show that the SNe in our sample follow the analytic result from (Shussman et al. 2016a), that the flux on the RJ tail follows $F_\nu \propto \nu^{1.4}$.

SN name	$\alpha_{T,early}$	$\alpha_{T,late}$	$\alpha_{L,early}$	$\alpha_{L,late}$
SN1999em	-0.34 (0.06)$^{+0.18}_{-0.16}$	-0.05 (0.04)$^{+0.00}_{-0.00}$	-0.54 (0.09)$^{+0.28}_{-0.25}$	-0.06 (0.06)$^{+0.01}_{-0.01}$
SN2004et	-0.21 (0.12)$^{+0.01}_{-0.01}$	-0.11 (0.05)$^{+0.00}_{-0.00}$	-0.24 (0.17)$^{+0.01}_{-0.01}$	-0.24 (0.09)$^{+0.00}_{-0.00}$
SN2005cs	-0.47 (0.03)$^{+0.00}_{-0.00}$	-0.06 (0.07)$^{+0.00}_{-0.00}$	-0.68 (0.05)$^{+0.00}_{-0.00}$	0.13 (0.10)$^{+0.00}_{-0.00}$
SN2006bp	-0.27 (0.01)$^{+0.03}_{-0.03}$		-0.04 (0.01)$^{+0.01}_{-0.01}$	
SN2007od	-0.10 (0.27)$^{+0.06}_{-0.06}$	-0.09 (0.06)$^{+0.01}_{-0.01}$	-0.22 (0.29)$^{+0.14}_{-0.14}$	-0.81 (0.09)$^{+0.12}_{-0.12}$
SN2008in	-0.28 (0.10)$^{+0.28}_{-0.26}$	-0.07 (0.07)$^{+0.01}_{-0.01}$	-0.50 (0.12)$^{+0.49}_{-0.46}$	-0.52 (0.07)$^{+0.09}_{-0.09}$
SN2009N	-0.48 (0.22)$^{+0.35}_{-0.34}$	-0.07 (0.05)$^{+0.01}_{-0.01}$	-0.21 (0.19)$^{+0.15}_{-0.15}$	0.11 (0.05)$^{+0.02}_{-0.02}$
SN2009bw	-0.67 (0.05)$^{+0.23}_{-0.21}$	-0.04 (0.19)$^{+0.00}_{-0.00}$	-0.79 (0.07)$^{+0.25}_{-0.24}$	-0.29 (0.10)$^{+0.01}_{-0.01}$
SN2009ib	-0.29 (0.12)$^{+0.16}_{-0.15}$	-0.14 (0.08)$^{+0.02}_{-0.02}$	-0.32 (0.15)$^{+0.18}_{-0.17}$	-0.03 (0.05)$^{+0.00}_{-0.00}$
SN2012A	-0.84 (0.11)$^{+0.38}_{-0.37}$	-0.09 (0.06)$^{+0.01}_{-0.01}$	-1.07 (0.18)$^{+0.48}_{-0.47}$	-0.87 (0.07)$^{+0.06}_{-0.06}$
SN2012aw	-0.35 (0.02)$^{+0.02}_{-0.02}$	-0.11 (0.04)$^{+0.00}_{-0.00}$	-0.33 (0.03)$^{+0.02}_{-0.02}$	-0.09 (0.06)$^{+0.00}_{-0.00}$
SN2012ec	-0.50 (0.21)$^{+0.39}_{-0.38}$	-0.11 (0.07)$^{+0.02}_{-0.02}$	-0.75 (0.22)$^{+0.58}_{-0.56}$	-0.06 (0.13)$^{+0.01}_{-0.01}$
SN2013ab	-0.56 (0.02)$^{+0.07}_{-0.07}$		-0.80 (0.03)$^{+0.10}_{-0.10}$	
SN2013by	-0.30 (0.01)$^{+0.38}_{-0.84}$		-0.42 (0.01)$^{+0.49}_{-1.03}$	
SN2013ej	-0.21 (0.03)$^{+0.04}_{-0.03}$		-0.00 (0.05)$^{+0.00}_{-0.00}$	

Table 3. The early and late logarithmic derivatives of the temperature and the bolometric luminosity. The values of $\alpha_{\rm T,early}$ and $\alpha_{\rm L,early}$ increase by ≈ 0.1 and ≈ 0.2 respectively, with an extinction value of E(B − V) = 0.1 mag.

ACKNOWLEDGEMENTS

This research was supported by the I-Core center of excellence of the CHE-ISF. TF and EN were partially supported by an ERC starting grant (GRB/SN), an ISF grant (1277/13) and an ISA grant.

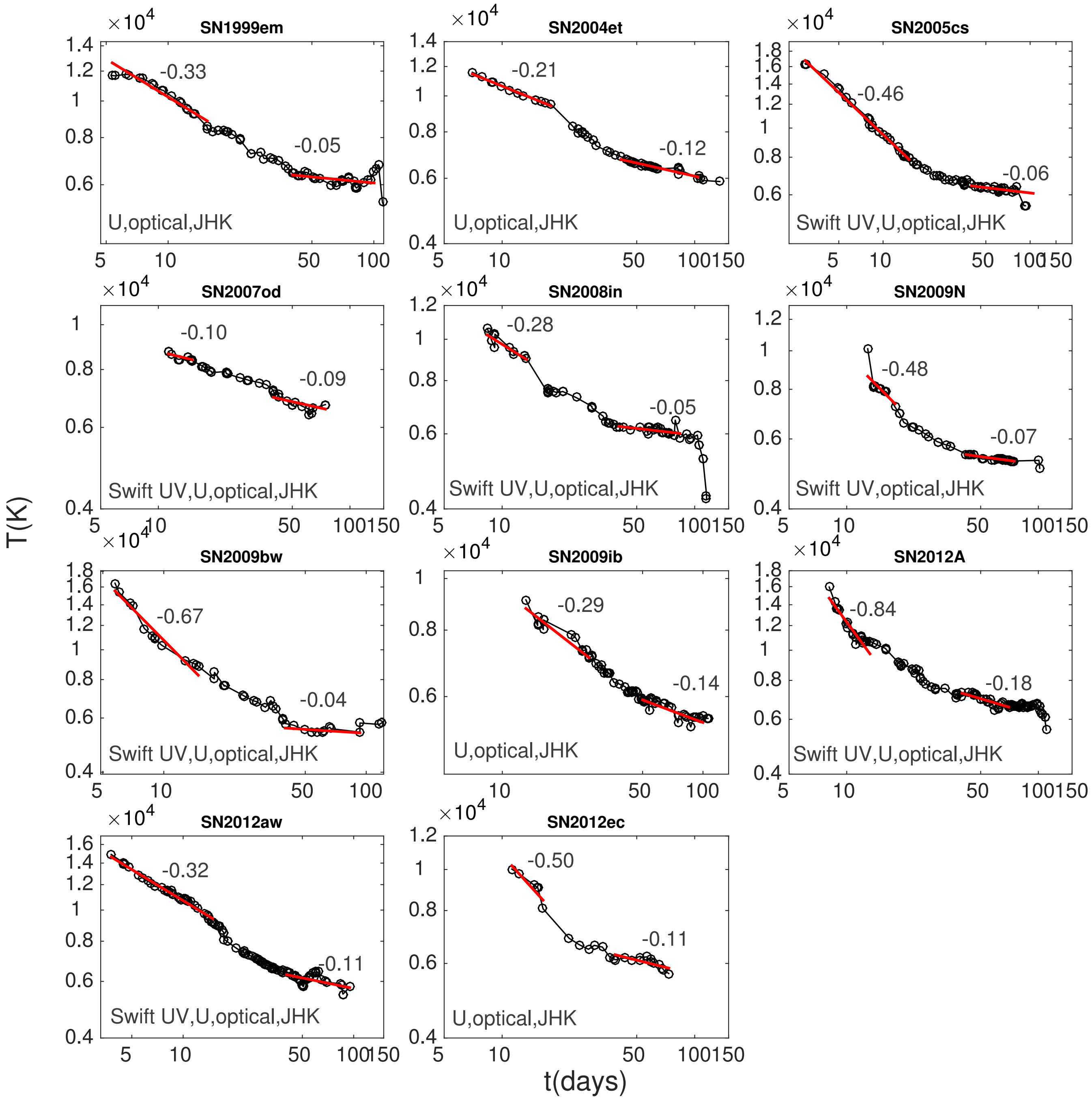

Figure 11. Temperature curves of objects that have both UV and JHK data. The numbers indicate the values of the best-fit early and late logarithmic derivative computed during the first 15 days, and during days 40-100 after the explosion, respectively. A clear flattening of the temperature is observed as the SN approcahes the temperaure of hydrogen recombination.

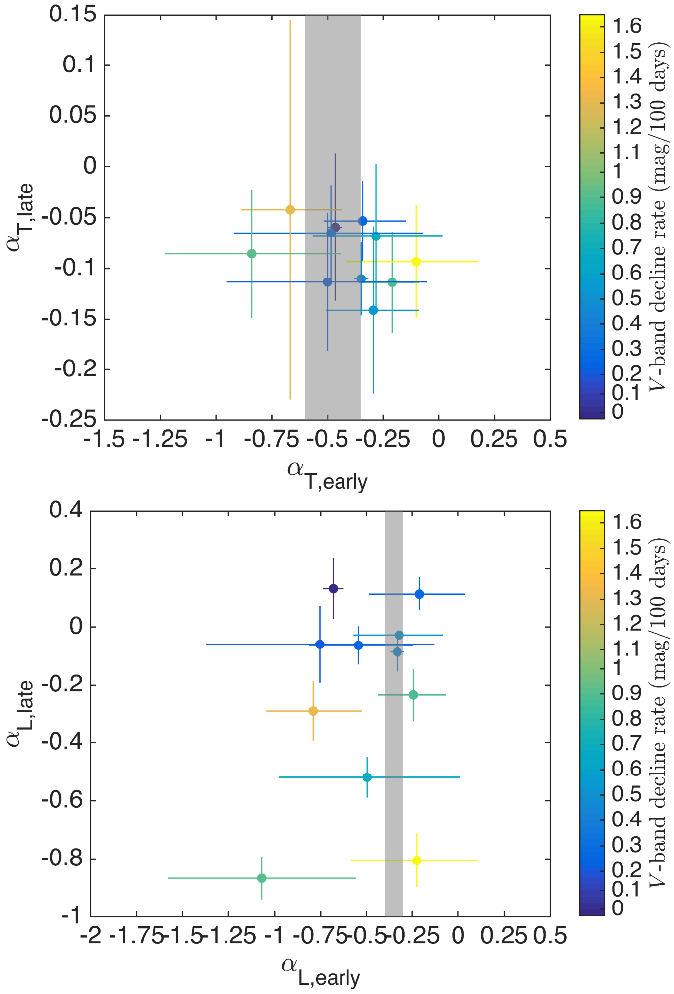

Figure 12. Top: the logarithmic derivative of the temperature at late times (40-100 days after the explosion) vs. the logarithmic derivative of the temperature at early times (up to 15 days after the explosion). The colors represent the decline rate of the V-band light curve. The values of the different objects agree with each other within the error-bars, and there is no apparent correlation with the light curve decline rate. Bottom: the same as the top figure for the bolometric luminosity. In this case, the early values of the logarithmic derivatives agree within the errors, but the late values show a wider spread. SNe whose luminosity declines faster at late phases (i.e., during the plateau phase) have faster declining light curves.

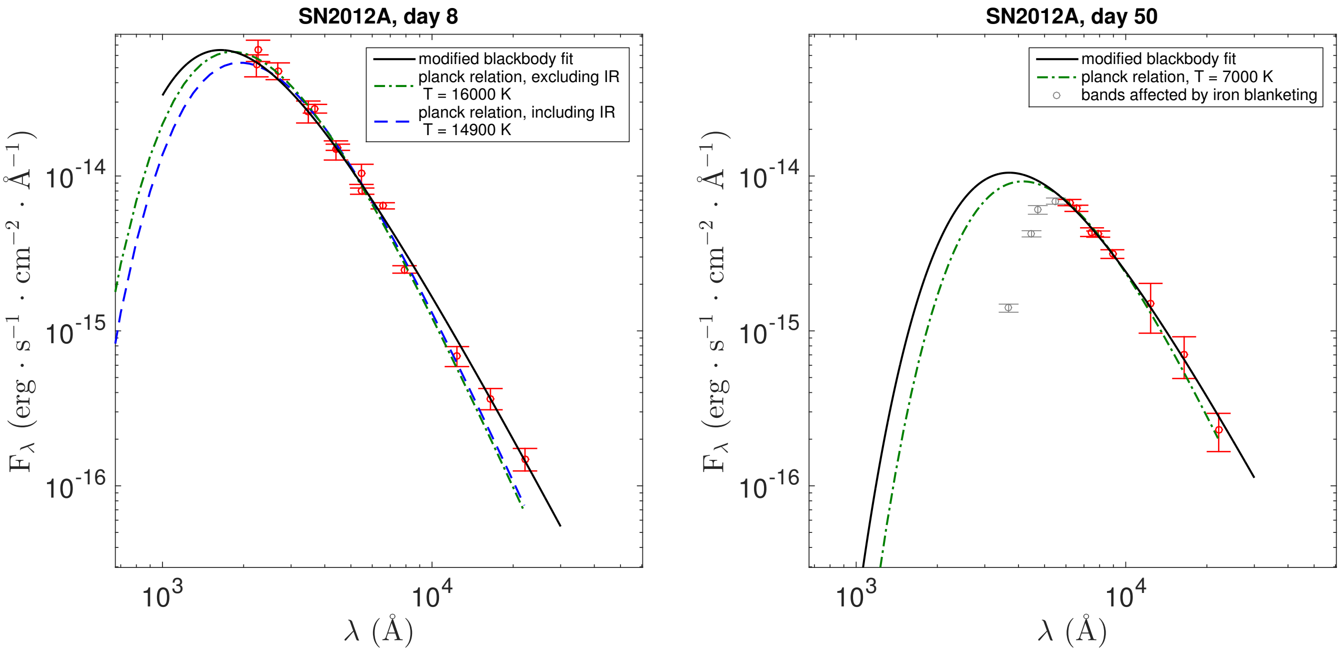

Figure 13. left:The SED of SN2012A at 8 days after the explosion. The standard Planck formula is only able to fit the peak of the distribution, but fails to fit the RJ tail. A modified black body model from Shussman et al. (2016a) is shown to be compatible throughout the whole wavelength range. right: An SED of SN2012A at 50 days past explosion. At this stage, after the onset of recombination and at low temperatures, both the modified black body and the standard model are able to describe the data.

REFERENCES

Anderson J. P., et al., 2014, ApJ, 786, 67
Arcavi I., et al., 2012, ApJ, 756, L30
Arnett W. D., 1980, ApJ, 237, 541
Barbarino C., et al., 2015, MNRAS, 448, 2312
Bersten M. C., Hamuy M., 2009, ApJ, 701, 200
Bose S., et al., 2013, MNRAS, 433, 1871
Bose S., et al., 2015a, MNRAS, 450, 2373
Bose S., et al., 2015b, ApJ, 806, 160
Cardelli J. A., Clayton G. C., Mathis J. S., 1989, ApJ, 345, 245
Dall'Ora M., et al., 2014, ApJ, 787, 139
Eastman R. G., Schmidt B. P., Kirshner R., 1996, ApJ, 466, 911
Falk S. W., Arnett W. D., 1977, ApJS, 33, 515
Faran T., et al., 2014a, MNRAS, 442, 844
Faran T., et al., 2014b, MNRAS, 445, 554
Fraser M., et al., 2011, MNRAS, 417, 1417
Gurugubelli U. K., Sahu D. K., Anupama G. C., Chakradhari N. K., 2008, Bulletin of the Astronomical Society of India, 36, 79
Hendry M. A., et al., 2006, MNRAS, 369, 1303
Inserra C., et al., 2011, MNRAS, 417, 261
Inserra C., et al., 2012, MNRAS, 422, 1122
Kasen D., Woosley S. E., 2009, ApJ, 703, 2205
Leonard D. C., et al., 2002a, PASP, 114, 35
Leonard D. C., et al., 2002b, AJ, 124, 2490
Lusk J. A., 2016, SuperBoL: Module for calculating the bolometric luminosities of supernovae, Astrophysics Source Code Library (ascl:1609.019)
Maguire K., et al., 2010, MNRAS, 404, 981
Nakar E., Sari R., 2010, ApJ, 725, 904
Nakar E., Poznanski D., Katz B., 2016, ApJ, 823, 127
Pastorello A., et al., 2009, MNRAS, 394, 2266
Patat F., Barbon R., Cappellaro E., Turatto M., 1994, A&A, 282, 731
Pejcha O., Prieto J. L., 2015, ApJ, 799, 215
Pinto P. A., Eastman R. G., 2000, ApJ, 530, 757
Quimby R. M., Wheeler J. C., Höflich P., Akerlof C. W., Brown P. J., Rykoff E. S., 2007, ApJ, 666, 1093
Rabinak I., Waxman E., 2011, ApJ, 728, 63
Richmond M. W., 2014, Journal of the American Association of Variable Star Observers (JAAVSO), 42, 333
Roy R., Kumar B., 2012, in Astronomical Society of India Conference Series. p. 115
Shussman T., Waldman R., Nakar E., 2016a, preprint, (arXiv:1610.05323)
Shussman T., Nakar E., Waldman R., Katz B., 2016b, preprint, (arXiv:1602.02774)
Smartt S. J., 2015, Publ. Astron. Soc. Australia, 32, e016
Takáts K., et al., 2014, MNRAS, 438, 368
Takáts K., et al., 2015, MNRAS, 450, 3137
Tomasella L., et al., 2013, MNRAS, 434, 1636
Tominaga N., Morokuma T., Blinnikov S. I., Baklanov P., Sorokina E. I., Nomoto K., 2011, ApJS, 193, 20
Utrobin V. P., 2007, A&A, 461, 233
Valenti S., et al., 2014, MNRAS, 438, L101
Valenti S., et al., 2015, MNRAS, 448, 2608
Valenti S., et al., 2016, MNRAS, 459, 3939
Van Dyk S. D., Li W., Filippenko A. V., 2003a, PASP, 115, 448
Van Dyk S. D., Li W., Filippenko A. V., 2003b, PASP, 115, 1289
Van Dyk S. D., et al., 2012, ApJ, 756, 131
Young T. R., 2004, ApJ, 617, 1233

APPENDIX A: A LIST OF THE TEMPERATURES AND BOLOMETRIC LUMINOSITIES

This paper has been typeset from a TEX/LATEX file prepared by the author.

Table A1. A List of the Temperatures and Bolometric Luminosities

MJD	$t - t_{\mathrm{explosion}}$	T(K)	L(10^{42} erg $\cdot s^{-1}$)
SN1999em			
51481	5	11670^{904}_{761}	$1.43^{0.19}_{0.14}$
51482	6	11748^{841}_{707}	$1.53^{0.17}_{0.15}$
51483	7	11493^{652}_{597}	$1.50^{0.14}_{0.12}$
51484	8	11075^{632}_{532}	$1.42^{0.13}_{0.10}$
51485	9	10681^{576}_{529}	$1.35^{0.11}_{0.09}$
51486	10	10320^{506}_{441}	$1.27^{0.09}_{0.07}$
51487	11	9944^{527}_{432}	$1.19^{0.09}_{0.07}$
51488	12	9539^{415}_{381}	$1.13^{0.06}_{0.05}$
51489	13	9250^{379}_{336}	$1.08^{0.05}_{0.05}$
51491	15	8481^{356}_{236}	$1.00^{0.04}_{0.04}$
51492	16	8300^{272}_{251}	$0.97^{0.06}_{0.06}$
51493	17	8340^{253}_{220}	$0.99^{0.06}_{0.05}$
51494	18	8340^{234}_{237}	$1.00^{0.05}_{0.05}$
51495	19	8310^{245}_{239}	$0.99^{0.05}_{0.05}$
51496	20	8160^{231}_{228}	$0.96^{0.05}_{0.05}$
51498	22	7899^{260}_{255}	$0.90^{0.05}_{0.05}$
51501	25	7250^{176}_{181}	$0.86^{0.04}_{0.04}$
51504	28	7320^{174}_{178}	$0.85^{0.04}_{0.03}$
51505	29	7040^{162}_{161}	$0.83^{0.03}_{0.03}$
51507	31	7060^{162}_{162}	$0.83^{0.03}_{0.03}$
51508	32	7040^{165}_{158}	$0.83^{0.03}_{0.03}$
51510	34	6950^{173}_{166}	$0.81^{0.03}_{0.03}$
51513	37	6740^{149}_{144}	$0.80^{0.03}_{0.03}$
51514	38	6600^{138}_{141}	$0.81^{0.03}_{0.03}$
51516	40	6440^{137}_{131}	$0.82^{0.03}_{0.03}$
51518	42	6340^{124}_{131}	$0.80^{0.03}_{0.03}$
51519	43	6320^{130}_{124}	$0.80^{0.03}_{0.02}$
51520	44	6360^{139}_{120}	$0.80^{0.03}_{0.02}$
51522	46	6480^{136}_{132}	$0.82^{0.03}_{0.03}$
51523	47	6460^{135}_{132}	$0.83^{0.03}_{0.03}$
51526	50	6300^{132}_{121}	$0.82^{0.03}_{0.03}$
51527	51	6260^{125}_{124}	$0.81^{0.03}_{0.03}$
51528	52	6260^{138}_{113}	$0.81^{0.03}_{0.02}$
51530	54	6220^{126}_{119}	$0.81^{0.03}_{0.02}$
51538	62	6000^{115}_{112}	$0.80^{0.02}_{0.02}$
51541	65	6033^{224}_{137}	$0.80^{0.05}_{0.03}$
51546	70	6150^{179}_{168}	$0.83^{0.04}_{0.04}$
51547	71	6140^{172}_{165}	$0.83^{0.04}_{0.04}$
51551	75	6270^{187}_{172}	$0.83^{0.04}_{0.04}$
51556	80	6120^{165}_{161}	$0.81^{0.04}_{0.04}$
51557	81	5920^{312}_{277}	$0.76^{0.08}_{0.07}$

Table A1 – *continued* A List of the Temperatures and Bolometric Luminosities

51558	82	5891^{341}_{324}	$0.76^{0.09}_{0.08}$
51565	89	6080^{166}_{169}	$0.77^{0.04}_{0.04}$
51570	94	6200^{164}_{172}	$0.76^{0.03}_{0.04}$
51572	96	6200^{165}_{171}	$0.74^{0.03}_{0.03}$
51576	100	6480^{188}_{183}	$0.72^{0.04}_{0.03}$
51578	102	6600^{193}_{193}	$0.71^{0.04}_{0.04}$
51581	105	6780^{280}_{266}	$0.69^{0.04}_{0.04}$
51586	110	5400^{538}_{449}	$0.40^{0.08}_{0.06}$
51592	116	4960^{447}_{367}	$0.29^{0.05}_{0.04}$
51599	123	4960^{435}_{376}	$0.21^{0.04}_{0.03}$
51604	128	5500^{292}_{247}	$0.17^{0.02}_{0.01}$
51606	130	5620^{233}_{230}	$0.16^{0.01}_{0.01}$
51607	131	5620^{163}_{144}	$0.16^{0.01}_{0.01}$
51613	137	5640^{154}_{162}	$0.14^{0.01}_{0.01}$
51614	138	5640^{161}_{135}	$0.14^{0.01}_{0.01}$
51619	143	5760^{156}_{142}	$0.14^{0.01}_{0.01}$
51620	144	5760^{139}_{147}	$0.14^{0.01}_{0.01}$
51624	148	5920^{151}_{152}	$0.15^{0.01}_{0.01}$
51627	151	5900^{158}_{144}	$0.14^{0.01}_{0.01}$
51629	153	5940^{150}_{155}	$0.14^{0.01}_{0.01}$
51634	158	5960^{159}_{150}	$0.13^{0.01}_{0.01}$
51637	161	5880^{158}_{165}	$0.12^{0.01}_{0.01}$
51638	162	5160^{597}_{454}	$0.10^{0.02}_{0.01}$
51639	163	5460^{707}_{546}	$0.11^{0.03}_{0.02}$
51640	164	5300^{680}_{516}	$0.10^{0.03}_{0.02}$
51641	165	5024^{1549}_{518}	$0.09^{0.06}_{0.01}$
51642	166	5640^{774}_{602}	$0.11^{0.03}_{0.02}$
51643	167	5880^{671}_{531}	$0.11^{0.03}_{0.02}$
51644	168	5920^{751}_{561}	$0.12^{0.03}_{0.02}$
51650	174	5580^{595}_{472}	$0.09^{0.02}_{0.01}$
51653	177	5400^{534}_{450}	$0.08^{0.02}_{0.01}$
51655	179	6080^{727}_{571}	$0.10^{0.03}_{0.02}$
51656	180	5560^{580}_{475}	$0.08^{0.02}_{0.01}$
SN1999gi			
51524	5	8680^{752}_{611}	$0.57^{0.07}_{0.05}$
51525	6	8480^{347}_{323}	$0.59^{0.03}_{0.02}$
51528	9	8100^{307}_{298}	$0.65^{0.02}_{0.02}$
51529	10	7880^{291}_{280}	$0.63^{0.02}_{0.02}$
51530	11	7720^{276}_{269}	$0.63^{0.02}_{0.02}$
51531	12	7560^{269}_{253}	$0.62^{0.02}_{0.02}$
51534	15	7436^{700}_{307}	$0.60^{0.06}_{0.02}$
51540	21	6860^{411}_{389}	$0.59^{0.03}_{0.02}$
51545	26	6760^{419}_{360}	$0.56^{0.03}_{0.02}$

Table A1 – *continued* A List of the Temperatures and Bolometric Luminosities

51550	31	6120^{334}_{292}	$0.52^{0.02}_{0.02}$
51556	37	5920^{308}_{274}	$0.50^{0.01}_{0.01}$
51577	58	5320^{243}_{219}	$0.50^{0.01}_{0.01}$
51582	63	5260^{232}_{219}	$0.49^{0.01}_{0.01}$
51590	71	5080^{223}_{197}	$0.50^{0.02}_{0.02}$
51614	95	5140^{218}_{211}	$0.45^{0.02}_{0.01}$
51619	100	4960^{200}_{198}	$0.45^{0.02}_{0.01}$
51624	105	4880^{205}_{181}	$0.43^{0.02}_{0.01}$
51629	110	4880^{200}_{185}	$0.40^{0.01}_{0.01}$
51634	115	4700^{178}_{177}	$0.36^{0.02}_{0.01}$
51638	119	4580^{167}_{169}	$0.31^{0.01}_{0.01}$
51643	124	4220^{145}_{139}	$0.25^{0.01}_{0.01}$
51648	129	4060^{211}_{185}	$0.17^{0.02}_{0.01}$
51653	134	3760^{116}_{110}	$0.13^{0.01}_{0.01}$
51658	139	3300^{155}_{142}	$0.17^{0.03}_{0.02}$
51664	145	3640^{104}_{107}	$0.11^{0.01}_{0.01}$
51669	150	3620^{101}_{108}	$0.11^{0.01}_{0.01}$
SN2000dc			
51766	4	8540^{353}_{327}	$1.39^{0.06}_{0.06}$
51767	5	8220^{327}_{300}	$1.46^{0.06}_{0.05}$
51773	11	7100^{243}_{215}	$1.70^{0.05}_{0.04}$
51775	13	7020^{231}_{214}	$1.69^{0.05}_{0.04}$
51777	15	6940^{226}_{208}	$1.63^{0.04}_{0.04}$
51779	17	6800^{206}_{210}	$1.55^{0.04}_{0.04}$
51781	19	6540^{196}_{187}	$1.50^{0.03}_{0.04}$
SN2001cm			
52069	5	9580^{494}_{424}	$1.63^{0.11}_{0.09}$
52070	6	9840^{516}_{455}	$1.73^{0.12}_{0.10}$
52071	7	9960^{531}_{467}	$1.78^{0.13}_{0.10}$
52072	8	9780^{507}_{451}	$1.73^{0.11}_{0.10}$
52077	13	9280^{438}_{413}	$1.54^{0.09}_{0.08}$
52082	18	8300^{370}_{329}	$1.31^{0.06}_{0.05}$
52087	23	7440^{303}_{273}	$1.13^{0.04}_{0.04}$
SN2001cy			
52092	6	11400^{687}_{605}	$3.32^{0.33}_{0.27}$
52093	7	11140^{638}_{587}	$3.17^{0.29}_{0.24}$
52094	8	10920^{615}_{557}	$3.05^{0.27}_{0.22}$
52095	9	10720^{614}_{516}	$2.95^{0.26}_{0.20}$
52096	10	10620^{759}_{668}	$2.89^{0.34}_{0.27}$
52097	11	10480^{548}_{519}	$2.81^{0.22}_{0.19}$
52098	12	10200^{1115}_{886}	$2.68^{0.39}_{0.26}$
52099	13	10240^{535}_{480}	$2.66^{0.20}_{0.17}$

Table A1 – *continued* A List of the Temperatures and Bolometric Luminosities

52100	14	9878^{1460}_{522}	$2.48^{0.63}_{0.18}$
52102	16	10020^{1028}_{853}	$2.49^{0.42}_{0.30}$
52104	18	9680^{954}_{787}	$2.30^{0.36}_{0.26}$
52106	20	9460^{1017}_{812}	$2.17^{0.37}_{0.25}$
52112	26	8400^{699}_{568}	$1.65^{0.18}_{0.12}$
52117	31	7740^{553}_{495}	$1.38^{0.11}_{0.09}$
52122	36	7260^{500}_{422}	$1.22^{0.08}_{0.06}$
52132	46	6660^{402}_{356}	$1.06^{0.05}_{0.04}$
52137	51	6540^{389}_{336}	$1.02^{0.04}_{0.03}$
52142	56	6440^{379}_{322}	$0.98^{0.04}_{0.03}$
52147	61	6380^{357}_{326}	$0.94^{0.04}_{0.03}$
52152	66	6220^{338}_{309}	$0.90^{0.03}_{0.03}$
52157	71	6080^{327}_{290}	$0.88^{0.03}_{0.03}$
52162	76	5940^{323}_{273}	$0.87^{0.03}_{0.02}$
52167	81	5980^{320}_{276}	$0.86^{0.03}_{0.02}$
52172	86	6060^{318}_{294}	$0.83^{0.03}_{0.02}$
52177	91	5820^{291}_{269}	$0.77^{0.02}_{0.02}$
52182	96	5600^{276}_{242}	$0.71^{0.02}_{0.02}$
SN2001do			
52137	3	8780^{385}_{339}	$1.34^{0.07}_{0.06}$
52138	4	8117^{1077}_{362}	$1.29^{0.22}_{0.05}$
52139	5	8300^{682}_{551}	$1.42^{0.15}_{0.10}$
52140	6	7780^{574}_{490}	$1.36^{0.11}_{0.08}$
52141	7	7680^{544}_{486}	$1.36^{0.10}_{0.08}$
52142	8	7500^{514}_{462}	$1.35^{0.09}_{0.08}$
52145	11	7100^{452}_{412}	$1.34^{0.08}_{0.06}$
52148	14	6580^{387}_{345}	$1.28^{0.05}_{0.05}$
52151	17	6720^{409}_{359}	$1.19^{0.06}_{0.04}$
52154	20	6360^{370}_{312}	$1.14^{0.04}_{0.04}$
52157	23	6240^{332}_{318}	$1.07^{0.04}_{0.03}$
52160	26	6200^{347}_{298}	$1.03^{0.03}_{0.03}$
52163	29	5900^{303}_{274}	$0.99^{0.03}_{0.03}$
52166	32	5600^{271}_{245}	$0.93^{0.02}_{0.03}$
52169	35	5640^{273}_{251}	$0.87^{0.02}_{0.02}$
52172	38	5520^{258}_{241}	$0.81^{0.02}_{0.02}$
52175	41	5340^{239}_{227}	$0.77^{0.02}_{0.02}$
52181	47	5120^{218}_{208}	$0.69^{0.02}_{0.02}$
52184	50	5160^{228}_{206}	$0.67^{0.02}_{0.02}$
52187	53	4860^{210}_{174}	$0.65^{0.02}_{0.02}$
52190	56	4940^{202}_{192}	$0.60^{0.02}_{0.02}$
52193	59	4960^{197}_{200}	$0.58^{0.02}_{0.02}$
52198	64	4760^{199}_{168}	$0.57^{0.02}_{0.02}$
52203	69	4000^{254}_{239}	$0.69^{0.10}_{0.08}$

Table A1 – *continued* A List of the Temperatures and Bolometric Luminosities

SN2001fa			
52202	4	14820^{1262}_{1073}	$12.54^{2.21}_{1.66}$
52203	5	13500^{1011}_{879}	$11.47^{1.65}_{1.29}$
52204	6	11980^{774}_{671}	$9.75^{1.09}_{0.86}$
52205	7	11320^{682}_{591}	$9.22^{0.90}_{0.72}$
52206	8	10580^{583}_{510}	$8.46^{0.70}_{0.56}$
52207	9	9800^{479}_{441}	$7.38^{0.49}_{0.42}$
52208	10	9560^{458}_{414}	$6.97^{0.44}_{0.37}$
52209	11	9160^{416}_{377}	$6.38^{0.35}_{0.31}$
52217	19	7600^{283}_{246}	$3.72^{0.12}_{0.11}$
52218	20	7613^{609}_{419}	$3.30^{0.28}_{0.17}$
52219	21	7760^{788}_{662}	$3.20^{0.32}_{0.21}$
52221	23	7580^{542}_{461}	$2.98^{0.22}_{0.17}$
52223	25	7600^{532}_{474}	$2.67^{0.20}_{0.15}$
52228	30	7380^{507}_{438}	$2.33^{0.16}_{0.12}$
52231	33	6980^{432}_{399}	$2.20^{0.12}_{0.10}$
52250	52	6900^{440}_{376}	$1.85^{0.10}_{0.08}$
52278	80	5960^{478}_{407}	$0.53^{0.03}_{0.02}$
52283	85	5740^{1013}_{735}	$0.48^{0.05}_{0.04}$
52288	90	6380^{1337}_{920}	$0.46^{0.10}_{0.05}$
52293	95	5200^{811}_{597}	$0.33^{0.02}_{0.02}$
SN2001x			
51976	13	10840^{624}_{533}	$1.76^{0.16}_{0.12}$
51984	21	8669^{1259}_{419}	$1.30^{0.28}_{0.06}$
51989	26	8800^{933}_{759}	$1.34^{0.21}_{0.15}$
51995	32	7920^{594}_{512}	$1.17^{0.10}_{0.08}$
52000	37	7500^{526}_{453}	$1.11^{0.08}_{0.06}$
52005	42	7160^{473}_{411}	$1.08^{0.06}_{0.05}$
52012	49	6900^{424}_{388}	$1.05^{0.05}_{0.04}$
52017	54	6780^{421}_{363}	$1.04^{0.05}_{0.04}$
52022	59	6700^{392}_{367}	$1.03^{0.05}_{0.04}$
52027	64	6640^{402}_{346}	$1.00^{0.05}_{0.04}$
52032	69	6580^{392}_{342}	$1.00^{0.04}_{0.03}$
52040	77	6460^{363}_{338}	$0.97^{0.04}_{0.03}$
52045	82	6340^{345}_{328}	$0.95^{0.03}_{0.03}$
52050	87	6220^{350}_{300}	$0.92^{0.03}_{0.03}$
52055	92	6160^{340}_{295}	$0.88^{0.03}_{0.03}$
52060	97	6080^{318}_{297}	$0.81^{0.02}_{0.02}$
52068	105	5760^{295}_{255}	$0.66^{0.02}_{0.02}$
52074	111	5400^{241}_{235}	$0.50^{0.01}_{0.01}$
52081	118	4980^{205}_{197}	$0.34^{0.01}_{0.01}$
52089	126	4620^{187}_{167}	$0.24^{0.01}_{0.01}$
52096	133	4760^{253}_{222}	$0.20^{0.01}_{0.01}$

Table A1 – *continued* A List of the Temperatures and Bolometric Luminosities

52103	140	4500^{164}_{161}	$0.19^{0.01}_{0.01}$
52110	147	4580^{173}_{164}	$0.18^{0.01}_{0.01}$
SN2002gd			
52555	2	13120^{985}_{826}	$1.04^{0.15}_{0.11}$
52556	3	12340^{839}_{733}	$1.02^{0.12}_{0.10}$
52559	6	10080^{522}_{477}	$0.99^{0.07}_{0.06}$
52562	9	8640^{441}_{378}	$0.77^{0.05}_{0.04}$
52570	17	8580^{1633}_{1118}	$0.74^{0.23}_{0.12}$
52573	20	8680^{3030}_{1688}	$0.73^{0.44}_{0.15}$
52576	23	8280^{2067}_{1339}	$0.67^{0.26}_{0.11}$
52579	26	7940^{1297}_{983}	$0.61^{0.15}_{0.09}$
52582	29	7860^{1276}_{957}	$0.59^{0.14}_{0.08}$
52585	32	7880^{1283}_{962}	$0.57^{0.13}_{0.08}$
52590	37	8180^{8162}_{2548}	$0.61^{1.60}_{0.19}$
52598	45	7420^{1121}_{846}	$0.56^{0.11}_{0.06}$
52608	55	6840^{928}_{715}	$0.51^{0.08}_{0.04}$
52613	60	6880^{1155}_{855}	$0.51^{0.09}_{0.05}$
52618	65	6900^{1388}_{955}	$0.52^{0.11}_{0.05}$
52634	81	6460^{795}_{648}	$0.43^{0.05}_{0.03}$
52659	106	5680^{1163}_{813}	$0.22^{0.03}_{0.01}$
52664	111	5300^{1800}_{1041}	$0.15^{0.04}_{0.01}$
SN2003hf			
52867	3	19000^{2873}_{2165}	$11.39^{4.17}_{2.54}$
52868	4	22940^{4454}_{3142}	$21.50^{11.31}_{6.09}$
52869	5	19820^{2926}_{2205}	$18.27^{6.68}_{4.11}$
52870	6	15560^{1442}_{1215}	$12.45^{2.48}_{1.82}$
52871	7	13960^{1121}_{958}	$11.19^{1.78}_{1.36}$
52872	8	13120^{1154}_{951}	$10.75^{1.73}_{1.25}$
52873	9	12180^{826}_{705}	$10.13^{1.20}_{0.95}$
52874	10	11820^{859}_{735}	$10.05^{1.21}_{0.93}$
52875	11	11380^{719}_{597}	$9.83^{1.02}_{0.78}$
52876	12	11040^{639}_{583}	$9.61^{0.89}_{0.74}$
52877	13	10660^{595}_{536}	$9.33^{0.79}_{0.66}$
52879	15	10040^{519}_{470}	$8.54^{0.62}_{0.52}$
52880	16	9740^{494}_{433}	$8.13^{0.55}_{0.46}$
52881	17	9420^{454}_{405}	$7.67^{0.47}_{0.40}$
52884	20	8641^{1025}_{415}	$6.51^{1.10}_{0.35}$
52886	22	8480^{702}_{594}	$6.14^{0.66}_{0.50}$
52888	24	7960^{601}_{522}	$5.41^{0.48}_{0.36}$
52890	26	7620^{552}_{468}	$4.80^{0.37}_{0.28}$
52892	28	7440^{612}_{506}	$4.29^{0.37}_{0.27}$
52894	30	7440^{581}_{508}	$3.91^{0.29}_{0.22}$
52896	32	7400^{522}_{462}	$3.58^{0.25}_{0.20}$

Table A1 – *continued* A List of the Temperatures and Bolometric Luminosities

52898	34	6980^{444}_{394}	$3.25^{0.18}_{0.14}$
52900	36	6700^{459}_{400}	$3.00^{0.15}_{0.12}$
52902	38	6505^{965}_{560}	$2.78^{0.41}_{0.17}$
52904	40	6660^{945}_{729}	$2.70^{0.38}_{0.21}$
52906	42	6740^{1007}_{765}	$2.60^{0.39}_{0.22}$
52910	46	6380^{896}_{671}	$2.40^{0.29}_{0.16}$
52913	49	6220^{936}_{723}	$2.31^{0.28}_{0.16}$
52919	55	6780^{1205}_{865}	$2.07^{0.40}_{0.21}$
SN2003hk			
52873	13	10500^{582}_{513}	$4.17^{0.35}_{0.28}$
52875	15	9600^{479}_{419}	$3.80^{0.25}_{0.21}$
52877	17	9360^{445}_{403}	$3.57^{0.21}_{0.19}$
52880	20	8660^{374}_{341}	$3.11^{0.15}_{0.13}$
52881	21	8680^{375}_{343}	$2.99^{0.15}_{0.12}$
52883	23	8720^{378}_{347}	$2.77^{0.14}_{0.12}$
52885	25	8507^{670}_{626}	$2.53^{0.26}_{0.21}$
52887	27	8580^{725}_{608}	$2.43^{0.27}_{0.20}$
52889	29	8280^{1191}_{878}	$2.29^{0.42}_{0.24}$
52893	33	8560^{1025}_{798}	$2.22^{0.39}_{0.26}$
52900	40	7620^{681}_{590}	$1.63^{0.18}_{0.13}$
52903	43	7260^{482}_{433}	$1.50^{0.10}_{0.07}$
52906	46	7140^{467}_{415}	$1.42^{0.08}_{0.07}$
52910	50	6760^{422}_{362}	$1.30^{0.06}_{0.05}$
52913	53	6480^{377}_{336}	$1.20^{0.05}_{0.04}$
52916	56	6500^{390}_{330}	$1.16^{0.05}_{0.04}$
52919	59	6480^{372}_{340}	$1.14^{0.05}_{0.04}$
52922	62	6460^{470}_{391}	$1.14^{0.06}_{0.05}$
52928	68	5440^{358}_{311}	$1.07^{0.04}_{0.04}$
52931	71	5960^{320}_{293}	$1.00^{0.03}_{0.03}$
52935	75	5840^{299}_{286}	$0.93^{0.03}_{0.03}$
52943	83	5300^{331}_{294}	$0.79^{0.03}_{0.03}$
52948	88	5760^{429}_{380}	$0.75^{0.03}_{0.03}$
SN2003iq			
52922	2	12940^{932}_{819}	$1.84^{0.25}_{0.20}$
52927	7	9620^{460}_{438}	$1.83^{0.12}_{0.10}$
52930	10	9260^{437}_{392}	$1.72^{0.10}_{0.09}$
52933	13	8700^{376}_{345}	$1.54^{0.07}_{0.07}$
52936	16	8111^{601}_{563}	$1.45^{0.13}_{0.11}$
52939	19	8080^{619}_{543}	$1.49^{0.14}_{0.11}$
52942	22	7880^{598}_{503}	$1.45^{0.12}_{0.09}$
52945	25	7680^{572}_{470}	$1.38^{0.11}_{0.08}$
52948	28	7560^{541}_{463}	$1.32^{0.10}_{0.07}$
52955	35	6680^{415}_{350}	$1.21^{0.06}_{0.04}$

Table A1 – *continued* A List of the Temperatures and Bolometric Luminosities

52960	40	6280^{430}_{377}	$1.20^{0.04}_{0.04}$
52963	43	6860^{437}_{372}	$1.19^{0.06}_{0.05}$
52966	46	6520^{373}_{348}	$1.15^{0.05}_{0.04}$
52969	49	6540^{398}_{332}	$1.13^{0.05}_{0.04}$
52972	52	6240^{352}_{305}	$1.13^{0.04}_{0.03}$
52977	57	5560^{329}_{284}	$1.15^{0.04}_{0.03}$
52992	72	6000^{309}_{292}	$0.99^{0.03}_{0.03}$
52996	76	5980^{324}_{276}	$0.94^{0.03}_{0.03}$
53002	82	5980^{307}_{290}	$0.88^{0.03}_{0.02}$
53017	97	5580^{1170}_{802}	$0.56^{0.06}_{0.04}$
53023	103	5020^{232}_{216}	$0.38^{0.02}_{0.01}$
53026	106	5040^{224}_{193}	$0.29^{0.01}_{0.01}$
53042	122	5120^{555}_{461}	$0.20^{0.01}_{0.01}$
53045	125	4620^{256}_{223}	$0.20^{0.01}_{0.01}$
53048	128	4520^{206}_{203}	$0.20^{0.01}_{0.01}$
SN2003z			
52670	5	12020^{783}_{698}	$0.22^{0.03}_{0.02}$
52671	6	12300^{831}_{729}	$0.24^{0.03}_{0.02}$
52674	9	10320^{556}_{497}	$0.19^{0.01}_{0.01}$
52676	11	9520^{467}_{414}	$0.17^{0.01}_{0.01}$
52679	14	8740^{1802}_{477}	$0.15^{0.05}_{0.01}$
52691	26	7200^{755}_{606}	$0.12^{0.01}_{0.01}$
52694	29	7380^{506}_{443}	$0.12^{0.01}_{0.01}$
52701	36	7180^{473}_{419}	$0.13^{0.01}_{0.01}$
52704	39	7040^{448}_{405}	$0.12^{0.01}_{0.01}$
52707	42	6700^{412}_{355}	$0.12^{0.01}_{0.00}$
52712	47	7560^{681}_{574}	$0.15^{0.02}_{0.01}$
52717	52	6860^{1378}_{954}	$0.14^{0.03}_{0.02}$
52722	57	6280^{781}_{606}	$0.12^{0.01}_{0.01}$
52727	62	5900^{306}_{275}	$0.12^{0.00}_{0.00}$
52734	69	6220^{351}_{324}	$0.12^{0.00}_{0.00}$
52739	74	5600^{262}_{256}	$0.11^{0.00}_{0.00}$
52751	86	6180^{4384}_{1707}	$0.11^{0.04}_{0.01}$
52766	101	4840^{824}_{605}	$0.10^{0.01}_{0.01}$
52771	106	5640^{323}_{290}	$0.09^{0.00}_{0.00}$
52778	113	5900^{315}_{289}	$0.07^{0.00}_{0.00}$
SN2004A			
53018	11	7960^{369}_{337}	$1.06^{0.04}_{0.04}$
53032	25	6360^{197}_{192}	$0.90^{0.02}_{0.02}$
53037	30	6022^{592}_{510}	$0.87^{0.03}_{0.03}$
53045	38	5860^{529}_{438}	$0.88^{0.04}_{0.03}$
53050	43	5860^{409}_{348}	$0.89^{0.03}_{0.03}$
53052	45	5900^{329}_{297}	$0.89^{0.03}_{0.02}$

Table A1 – *continued* A List of the Temperatures and Bolometric Luminosities

53065	58	5740^{309}_{282}	$0.90^{0.02}_{0.02}$
53066	59	5760^{320}_{276}	$0.91^{0.02}_{0.02}$
53076	69	5700^{300}_{281}	$0.91^{0.02}_{0.02}$
53081	74	5710^{309}_{277}	$0.90^{0.03}_{0.03}$
53099	92	5620^{302}_{264}	$0.82^{0.02}_{0.02}$
SN2004du			
53231	3	14644^{2903}_{1658}	$4.53^{1.64}_{0.75}$
53233	5	11420^{700}_{620}	$3.61^{0.36}_{0.30}$
53235	7	10140^{539}_{475}	$3.35^{0.25}_{0.21}$
53237	9	9500^{458}_{418}	$3.21^{0.20}_{0.17}$
53239	11	9120^{419}_{381}	$3.06^{0.17}_{0.15}$
53242	14	8900^{397}_{361}	$2.93^{0.15}_{0.13}$
53244	16	8680^{370}_{347}	$2.70^{0.13}_{0.11}$
53246	18	8500^{457}_{415}	$2.55^{0.14}_{0.12}$
53250	22	8153^{707}_{499}	$2.31^{0.25}_{0.15}$
53251	23	8160^{650}_{542}	$2.26^{0.22}_{0.16}$
53253	25	8120^{625}_{549}	$2.21^{0.20}_{0.16}$
53255	27	8040^{611}_{537}	$2.18^{0.20}_{0.15}$
53257	29	7920^{610}_{505}	$2.13^{0.19}_{0.14}$
53259	31	7780^{590}_{483}	$2.07^{0.17}_{0.13}$
53263	35	7480^{517}_{460}	$1.94^{0.14}_{0.11}$
53265	37	7320^{495}_{437}	$1.88^{0.12}_{0.10}$
53267	39	7180^{489}_{407}	$1.82^{0.12}_{0.08}$
53269	41	7120^{465}_{411}	$1.79^{0.11}_{0.08}$
53271	43	7060^{462}_{400}	$1.75^{0.10}_{0.08}$
53273	45	7160^{678}_{553}	$1.78^{0.17}_{0.11}$
53276	48	6760^{449}_{406}	$1.65^{0.09}_{0.07}$
53279	51	6420^{373}_{326}	$1.58^{0.06}_{0.05}$
53282	54	6380^{366}_{323}	$1.57^{0.06}_{0.05}$
53285	57	6360^{366}_{319}	$1.55^{0.06}_{0.05}$
53288	60	6320^{344}_{328}	$1.53^{0.05}_{0.05}$
53292	64	6180^{338}_{304}	$1.51^{0.05}_{0.04}$
53301	73	5780^{362}_{325}	$1.47^{0.05}_{0.04}$
53309	81	5980^{321}_{279}	$1.41^{0.04}_{0.04}$
53329	101	5340^{316}_{290}	$1.26^{0.04}_{0.04}$
SN2004et			
53278	7	11580^{772}_{677}	$2.42^{0.27}_{0.22}$
53279	8	11280^{715}_{648}	$2.39^{0.25}_{0.21}$
53280	9	10900^{664}_{600}	$2.30^{0.22}_{0.18}$
53281	10	10620^{648}_{548}	$2.22^{0.21}_{0.16}$
53282	11	10380^{610}_{525}	$2.15^{0.19}_{0.15}$
53283	12	10140^{562}_{512}	$2.09^{0.17}_{0.14}$
53284	13	10020^{545}_{500}	$2.06^{0.16}_{0.14}$

Table A1 – *continued* A List of the Temperatures and Bolometric Luminosities

53286	15	9750^{538}_{473}	$2.00^{0.15}_{0.12}$
53287	16	9680^{507}_{462}	$1.98^{0.14}_{0.12}$
53288	17	9600^{506}_{447}	$1.97^{0.14}_{0.11}$
53289	18	9500^{500}_{432}	$1.96^{0.14}_{0.11}$
53294	23	8300^{201}_{195}	$1.65^{0.06}_{0.06}$
53296	25	8021^{411}_{235}	$1.57^{0.14}_{0.07}$
53297	26	7989^{306}_{264}	$1.58^{0.10}_{0.08}$
53298	27	7880^{248}_{235}	$1.55^{0.08}_{0.07}$
53299	28	7760^{239}_{209}	$1.51^{0.08}_{0.07}$
53301	30	7600^{214}_{213}	$1.46^{0.07}_{0.06}$
53302	31	7340^{212}_{185}	$1.42^{0.07}_{0.06}$
53306	35	7120^{169}_{162}	$1.35^{0.05}_{0.05}$
53307	36	7040^{170}_{153}	$1.32^{0.05}_{0.05}$
53309	38	6960^{172}_{145}	$1.30^{0.05}_{0.04}$
53312	41	6860^{160}_{146}	$1.27^{0.05}_{0.04}$
53315	44	6740^{141}_{152}	$1.23^{0.04}_{0.04}$
53316	45	6700^{140}_{149}	$1.22^{0.04}_{0.04}$
53317	46	6660^{141}_{144}	$1.20^{0.04}_{0.04}$
53318	47	6640^{140}_{143}	$1.20^{0.04}_{0.04}$
53319	48	6610^{153}_{144}	$1.19^{0.04}_{0.04}$
53320	49	6590^{146}_{141}	$1.19^{0.04}_{0.04}$
53324	53	6520^{244}_{153}	$1.18^{0.08}_{0.04}$
53326	55	6520^{197}_{180}	$1.19^{0.06}_{0.06}$
53327	56	6500^{196}_{178}	$1.18^{0.21}_{0.11}$
53328	57	6480^{194}_{179}	$1.18^{0.06}_{0.06}$
53329	58	6480^{197}_{177}	$1.18^{0.06}_{0.06}$
53330	59	6480^{187}_{186}	$1.18^{0.06}_{0.06}$
53331	60	6450^{192}_{187}	$1.17^{0.06}_{0.06}$
53332	61	6420^{191}_{177}	$1.16^{0.06}_{0.06}$
53333	62	6400^{192}_{173}	$1.16^{0.06}_{0.06}$
53335	64	6360^{186}_{181}	$1.14^{0.06}_{0.05}$
53350	79	6480^{256}_{242}	$1.13^{0.33}_{0.15}$
53353	82	6266^{395}_{260}	$1.08^{0.08}_{0.07}$
53354	83	6340^{219}_{211}	$1.08^{0.06}_{0.05}$
53355	84	6320^{234}_{196}	$1.08^{0.06}_{0.05}$
53375	104	6020^{162}_{153}	$0.84^{0.06}_{0.05}$
53376	105	6080^{160}_{161}	$0.83^{0.08}_{0.05}$
53378	107	6020^{162}_{153}	$0.78^{0.06}_{0.04}$
53381	110	5920^{147}_{156}	$0.71^{0.26}_{0.14}$
53406	135	5880^{205}_{194}	$0.20^{0.07}_{0.04}$
53412	141	5940^{214}_{203}	$0.17^{0.04}_{0.04}$
SN2005cs			
53552	3	16327^{745}_{684}	$0.89^{0.08}_{0.07}$
53553	4	15060^{801}_{749}	$0.78^{0.08}_{0.07}$

Table A1 – *continued* A List of the Temperatures and Bolometric Luminosities

53554	5	13509^{693}_{623}	$0.63^{0.06}_{0.05}$
53555	6	12356^{846}_{692}	$0.54^{0.06}_{0.04}$
53557	8	10418^{788}_{668}	$0.42^{0.03}_{0.03}$
53558	9	9690^{317}_{298}	$0.38^{0.02}_{0.02}$
53559	10	9540^{295}_{271}	$0.38^{0.02}_{0.02}$
53560	11	9269^{374}_{364}	$0.36^{0.02}_{0.02}$
53562	13	8376^{468}_{333}	$0.31^{0.03}_{0.02}$
53563	14	8088^{246}_{230}	$0.30^{0.02}_{0.02}$
53564	15	7967^{247}_{220}	$0.29^{0.02}_{0.01}$
53565	16	7708^{242}_{219}	$0.27^{0.01}_{0.01}$
53566	17	7560^{242}_{217}	$0.27^{0.01}_{0.01}$
53568	19	7360^{195}_{191}	$0.26^{0.01}_{0.01}$
53569	20	7260^{200}_{175}	$0.25^{0.01}_{0.01}$
53571	22	6960^{192}_{177}	$0.24^{0.01}_{0.01}$
53572	23	6920^{186}_{178}	$0.24^{0.01}_{0.01}$
53573	24	6967^{175}_{176}	$0.24^{0.01}_{0.01}$
53574	25	6880^{159}_{147}	$0.24^{0.01}_{0.01}$
53575	26	6700^{150}_{142}	$0.24^{0.01}_{0.01}$
53577	28	6720^{178}_{150}	$0.24^{0.01}_{0.01}$
53579	30	6670^{167}_{162}	$0.24^{0.01}_{0.01}$
53580	31	6760^{204}_{200}	$0.24^{0.01}_{0.01}$
53583	34	6660^{184}_{186}	$0.24^{0.01}_{0.01}$
53584	35	6604^{227}_{180}	$0.25^{0.01}_{0.01}$
53585	36	6505^{202}_{180}	$0.24^{0.01}_{0.01}$
53586	37	6700^{251}_{228}	$0.26^{0.01}_{0.01}$
53588	39	6560^{232}_{225}	$0.26^{0.01}_{0.01}$
53589	40	6500^{227}_{220}	$0.26^{0.01}_{0.01}$
53591	42	6360^{196}_{176}	$0.26^{0.01}_{0.01}$
53593	44	6360^{187}_{177}	$0.26^{0.02}_{0.01}$
53595	46	6360^{210}_{188}	$0.27^{0.02}_{0.02}$
53599	50	6360^{180}_{183}	$0.27^{0.01}_{0.01}$
53600	51	6340^{187}_{175}	$0.27^{0.01}_{0.01}$
53605	56	6250^{196}_{182}	$0.28^{0.02}_{0.01}$
53606	57	6360^{184}_{180}	$0.29^{0.01}_{0.01}$
53610	61	6203^{230}_{247}	$0.28^{0.02}_{0.02}$
53612	63	6260^{168}_{175}	$0.29^{0.01}_{0.01}$
53613	64	6320^{184}_{181}	$0.30^{0.01}_{0.01}$
53615	66	6310^{182}_{182}	$0.30^{0.01}_{0.01}$
53617	68	6220^{167}_{171}	$0.29^{0.01}_{0.01}$
53619	70	6200^{181}_{156}	$0.29^{0.01}_{0.01}$
53624	75	6100^{199}_{196}	$0.29^{0.01}_{0.01}$
53626	77	6240^{185}_{157}	$0.30^{0.01}_{0.01}$
53628	79	6220^{182}_{159}	$0.30^{0.01}_{0.01}$
53629	80	6400^{906}_{687}	$0.33^{0.01}_{0.01}$
53640	91	5520^{568}_{568}	$0.24^{0.01}_{0.01}$

Table A1 – *continued* A List of the Temperatures and Bolometric Luminosities

53642	93	5520^{583}_{460}	$0.24^{0.02}_{0.01}$
53781	232	4080^{338}_{283}	$0.01^{0.01}_{0.00}$
SN2006bp			
53836	2	10662^{480}_{632}	$0.90^{0.06}_{0.06}$
53837	3	9779^{267}_{208}	$0.91^{0.04}_{0.04}$
53838	4	9380^{163}_{152}	$0.95^{0.02}_{0.02}$
53839	5	8713^{171}_{215}	$0.97^{0.02}_{0.02}$
53840	6	8292^{225}_{173}	$0.97^{0.02}_{0.02}$
53841	7	8085^{158}_{155}	$0.96^{0.02}_{0.02}$
53842	8	7796^{175}_{169}	$0.95^{0.02}_{0.02}$
53843	9	7447^{150}_{135}	$0.93^{0.02}_{0.02}$
53844	10	7176^{156}_{269}	$0.92^{0.02}_{0.02}$
53846	12	6724^{143}_{130}	$0.89^{0.02}_{0.02}$
53847	13	6640^{124}_{126}	$0.88^{0.02}_{0.02}$
53848	14	6513^{169}_{170}	$0.87^{0.02}_{0.02}$
53849	15	6360^{231}_{215}	$0.85^{0.02}_{0.02}$
53850	16	6290^{203}_{190}	$0.84^{0.02}_{0.02}$
53852	18	6050^{181}_{186}	$0.84^{0.02}_{0.02}$
53854	20	5782^{467}_{198}	$0.83^{0.02}_{0.02}$
53857	23	5880^{365}_{313}	$0.84^{0.02}_{0.02}$
53858	24	5840^{345}_{314}	$0.84^{0.02}_{0.02}$
53859	25	5740^{338}_{298}	$0.84^{0.02}_{0.02}$
53860	26	5680^{335}_{291}	$0.83^{0.02}_{0.02}$
53861	27	5560^{314}_{285}	$0.83^{0.03}_{0.02}$
53862	28	5580^{312}_{292}	$0.83^{0.03}_{0.02}$
53866	32	5420^{297}_{273}	$0.81^{0.03}_{0.02}$
53867	33	5340^{294}_{253}	$0.81^{0.03}_{0.02}$
53870	36	5300^{271}_{264}	$0.78^{0.03}_{0.02}$
53886	52	4960^{248}_{229}	$0.74^{0.04}_{0.03}$
SN2007od			
54410	11	8720^{582}_{504}	$6.60^{0.37}_{0.31}$
54411	12	8640^{577}_{520}	$6.55^{0.36}_{0.32}$
54412	13	8420^{355}_{330}	$6.55^{0.32}_{0.29}$
54413	14	8500^{330}_{288}	$6.34^{0.30}_{0.24}$
54414	15	8386^{195}_{180}	$6.17^{0.37}_{0.25}$
54416	17	8140^{153}_{157}	$5.72^{0.22}_{0.21}$
54417	18	8000^{188}_{180}	$5.49^{0.24}_{0.24}$
54418	19	7904^{203}_{233}	$5.34^{0.26}_{0.29}$
54422	23	7846^{299}_{223}	$5.18^{0.45}_{0.28}$
54426	27	7680^{201}_{172}	$4.96^{0.23}_{0.19}$
54428	29	7600^{186}_{184}	$4.79^{0.21}_{0.20}$
54429	30	7580^{186}_{176}	$4.75^{0.21}_{0.19}$
54433	34	7500^{187}_{167}	$4.56^{0.19}_{0.18}$

Table A1 – *continued* A List of the Temperatures and Bolometric Luminosities

54436	37	7420^{201}_{192}	$4.46^{0.22}_{0.20}$
54439	40	7150^{245}_{232}	$4.12^{0.27}_{0.23}$
54441	42	7060^{161}_{168}	$3.99^{0.15}_{0.16}$
54442	43	7000^{145}_{154}	$3.91^{0.13}_{0.14}$
54446	47	6860^{137}_{148}	$3.70^{0.12}_{0.12}$
54449	50	6690^{149}_{146}	$3.46^{0.13}_{0.13}$
54450	51	6800^{146}_{152}	$3.54^{0.13}_{0.13}$
54451	52	6800^{149}_{155}	$3.54^{0.13}_{0.13}$
54456	57	6660^{184}_{167}	$3.40^{0.17}_{0.15}$
54460	61	6446^{319}_{190}	$3.05^{0.34}_{0.16}$
54462	63	6440^{128}_{138}	$2.96^{0.10}_{0.10}$
54464	65	6600^{160}_{144}	$3.06^{0.12}_{0.11}$
54473	74	6720^{149}_{131}	$2.48^{0.09}_{0.08}$
SN2008in			
54830	8	10600^{193}_{168}	$0.70^{0.02}_{0.02}$
54831	9	9965^{741}_{560}	$0.64^{0.07}_{0.05}$
54833	11	9383^{519}_{456}	$0.57^{0.04}_{0.03}$
54835	13	9123^{401}_{399}	$0.54^{0.03}_{0.03}$
54839	17	7575^{371}_{285}	$0.44^{0.03}_{0.02}$
54841	19	7519^{312}_{282}	$0.45^{0.02}_{0.02}$
54843	21	7540^{345}_{307}	$0.44^{0.02}_{0.02}$
54846	24	7300^{338}_{303}	$0.42^{0.02}_{0.02}$
54851	29	6919^{354}_{275}	$0.40^{0.02}_{0.01}$
54855	33	6600^{284}_{256}	$0.38^{0.02}_{0.01}$
54856	34	6420^{212}_{203}	$0.37^{0.01}_{0.01}$
54858	36	6340^{192}_{183}	$0.36^{0.01}_{0.01}$
54860	38	6320^{183}_{185}	$0.36^{0.01}_{0.01}$
54861	39	6240^{175}_{149}	$0.36^{0.01}_{0.01}$
54862	40	6240^{198}_{170}	$0.36^{0.01}_{0.01}$
54864	42	6220^{185}_{176}	$0.36^{0.01}_{0.01}$
54868	46	6140^{205}_{181}	$0.36^{0.01}_{0.01}$
54874	52	6220^{266}_{261}	$0.35^{0.01}_{0.01}$
54878	56	6100^{243}_{206}	$0.34^{0.01}_{0.01}$
54879	57	6084^{396}_{241}	$0.34^{0.01}_{0.01}$
54880	58	6240^{227}_{212}	$0.34^{0.01}_{0.01}$
54883	61	6140^{229}_{197}	$0.33^{0.01}_{0.01}$
54884	62	6180^{213}_{195}	$0.33^{0.01}_{0.01}$
54885	63	6170^{226}_{212}	$0.33^{0.01}_{0.01}$
54886	64	6220^{299}_{267}	$0.33^{0.02}_{0.02}$
54888	66	6180^{302}_{258}	$0.32^{0.02}_{0.01}$
54889	67	6060^{197}_{182}	$0.31^{0.01}_{0.01}$
54890	68	6060^{208}_{190}	$0.31^{0.01}_{0.01}$
54893	71	6060^{209}_{206}	$0.30^{0.01}_{0.01}$
54895	73	6021^{232}_{238}	$0.30^{0.01}_{0.01}$

Table A1 – *continued* A List of the Temperatures and Bolometric Luminosities

54900	78	5940^{286}_{271}	$0.29^{0.01}_{0.01}$
54901	79	6460^{679}_{542}	$0.31^{0.03}_{0.02}$
54906	84	5880^{257}_{246}	$0.28^{0.01}_{0.01}$
54912	90	6000^{335}_{288}	$0.26^{0.01}_{0.01}$
54915	93	5840^{193}_{187}	$0.24^{0.01}_{0.01}$
54917	95	5860^{193}_{167}	$0.23^{0.01}_{0.01}$
54925	103	5960^{248}_{225}	$0.20^{0.01}_{0.01}$
54927	105	5649^{250}_{213}	$0.17^{0.01}_{0.00}$
54932	110	5240^{207}_{204}	$0.12^{0.00}_{0.00}$
54937	115	4279^{170}_{281}	$0.08^{0.00}_{0.00}$
SN2009N			
54858	13	10120^{835}_{711}	$0.57^{0.04}_{0.03}$
54859	14	8154^{256}_{259}	$0.53^{0.02}_{0.02}$
54860	15	8050^{236}_{220}	$0.53^{0.01}_{0.01}$
54861	16	7895^{232}_{217}	$0.52^{0.01}_{0.01}$
54863	18	7220^{154}_{143}	$0.50^{0.01}_{0.01}$
54864	19	6940^{148}_{142}	$0.49^{0.01}_{0.01}$
54865	20	6600^{138}_{123}	$0.49^{0.01}_{0.01}$
54867	22	6413^{120}_{97}	$0.47^{0.02}_{0.02}$
54869	24	6320^{135}_{134}	$0.47^{0.01}_{0.01}$
54871	26	6160^{132}_{121}	$0.46^{0.01}_{0.01}$
54872	27	6100^{118}_{130}	$0.46^{0.01}_{0.01}$
54875	30	5900^{123}_{113}	$0.46^{0.01}_{0.01}$
54878	33	5800^{148}_{124}	$0.47^{0.02}_{0.02}$
54880	35	5750^{140}_{130}	$0.48^{0.02}_{0.02}$
54887	42	5500^{122}_{118}	$0.49^{0.02}_{0.01}$
54888	43	5480^{126}_{113}	$0.50^{0.02}_{0.01}$
54889	44	5480^{125}_{116}	$0.50^{0.01}_{0.01}$
54890	45	5480^{114}_{124}	$0.50^{0.01}_{0.01}$
54891	46	5460^{120}_{117}	$0.51^{0.01}_{0.01}$
54896	51	5340^{123}_{104}	$0.52^{0.01}_{0.01}$
54897	52	5340^{123}_{103}	$0.52^{0.01}_{0.01}$
54902	57	5320^{115}_{109}	$0.53^{0.01}_{0.01}$
54904	59	5320^{123}_{101}	$0.53^{0.01}_{0.01}$
54906	61	5340^{114}_{112}	$0.54^{0.01}_{0.01}$
54907	62	5360^{113}_{115}	$0.53^{0.01}_{0.01}$
54908	63	5360^{113}_{114}	$0.53^{0.01}_{0.01}$
54909	64	5360^{112}_{116}	$0.53^{0.01}_{0.01}$
54910	65	5340^{109}_{116}	$0.54^{0.01}_{0.01}$
54911	66	5320^{124}_{101}	$0.54^{0.01}_{0.01}$
54913	68	5320^{112}_{114}	$0.54^{0.01}_{0.01}$
54915	70	5300^{119}_{104}	$0.53^{0.01}_{0.01}$
54916	71	5300^{112}_{110}	$0.53^{0.01}_{0.01}$
54917	72	5280^{123}_{100}	$0.53^{0.01}_{0.01}$

Table A1 – *continued* A List of the Temperatures and Bolometric Luminosities

54918	73	5280^{120}_{101}	$0.53^{0.01}_{0.01}$
54919	74	5280^{117}_{105}	$0.53^{0.01}_{0.01}$
54920	75	5280^{115}_{105}	$0.53^{0.01}_{0.01}$
54946	101	5300^{113}_{109}	$0.39^{0.01}_{0.01}$
54947	102	5060^{109}_{122}	$0.39^{0.01}_{0.01}$
SN2009bw			
54923	6	15826^{988}_{757}	$2.29^{0.64}_{0.09}$
54924	7	14043^{365}_{356}	$2.16^{0.08}_{0.08}$
54925	8	11720^{233}_{238}	$1.73^{0.06}_{0.05}$
54926	9	11022^{293}_{534}	$1.61^{0.08}_{0.10}$
54927	10	10360^{350}_{337}	$1.47^{0.06}_{0.06}$
54930	13	9240^{296}_{277}	$1.25^{0.05}_{0.04}$
54931	14	9040^{281}_{280}	$1.20^{0.04}_{0.04}$
54932	15	8891^{324}_{328}	$1.16^{0.05}_{0.05}$
54935	18	8324^{333}_{602}	$1.00^{0.04}_{0.07}$
54937	20	7638^{214}_{177}	$0.86^{0.02}_{0.02}$
54942	25	7090^{502}_{443}	$0.79^{0.05}_{0.04}$
54945	28	6820^{462}_{400}	$0.75^{0.04}_{0.03}$
54946	29	6780^{465}_{386}	$0.74^{0.04}_{0.03}$
54949	32	6500^{404}_{367}	$0.68^{0.03}_{0.03}$
54951	34	6840^{1744}_{1130}	$0.67^{0.19}_{0.08}$
54952	35	6560^{430}_{362}	$0.64^{0.03}_{0.02}$
54953	36	6400^{395}_{352}	$0.62^{0.03}_{0.02}$
54956	39	5950^{340}_{310}	$0.59^{0.02}_{0.02}$
54957	40	5760^{497}_{425}	$0.59^{0.02}_{0.02}$
54961	44	5680^{424}_{354}	$0.56^{0.02}_{0.02}$
54967	50	5480^{383}_{324}	$0.55^{0.02}_{0.02}$
54971	54	5420^{288}_{246}	$0.52^{0.02}_{0.02}$
54974	57	5420^{279}_{244}	$0.52^{0.01}_{0.01}$
54978	61	5400^{661}_{516}	$0.51^{0.03}_{0.04}$
54979	62	5460^{935}_{692}	$0.52^{0.04}_{0.03}$
54983	66	5600^{289}_{270}	$0.51^{0.01}_{0.01}$
54984	67	5540^{2929}_{1406}	$0.51^{0.23}_{0.05}$
55010	93	5450^{1079}_{295}	$0.45^{0.05}_{0.01}$
55033	116	5720^{731}_{581}	$0.36^{0.03}_{0.02}$
55037	120	5800^{765}_{590}	$0.34^{0.03}_{0.02}$
55040	123	5900^{1080}_{792}	$0.33^{0.04}_{0.02}$
55044	127	6236^{1920}_{1297}	$0.31^{0.10}_{0.03}$
55050	133	8500^{4925}_{2183}	$0.26^{0.32}_{0.07}$
SN2009ib			
55054	13	9120^{188}_{200}	$0.76^{0.02}_{0.02}$
55056	15	8192^{1031}_{351}	$0.67^{0.09}_{0.02}$
55057	16	8104^{1041}_{394}	$0.66^{0.14}_{0.04}$

Table A1 – *continued* A List of the Temperatures and Bolometric Luminosities

55063	22	7860^{626}_{519}	$0.65^{0.10}_{0.07}$
55064	23	7760^{590}_{496}	$0.64^{0.07}_{0.05}$
55066	25	7330^{543}_{444}	$0.60^{0.07}_{0.04}$
55067	26	7340^{512}_{453}	$0.60^{0.05}_{0.04}$
55068	27	7109^{509}_{409}	$0.57^{0.05}_{0.04}$
55069	28	7150^{479}_{410}	$0.59^{0.04}_{0.04}$
55070	29	6920^{420}_{379}	$0.55^{0.04}_{0.03}$
55071	30	6840^{415}_{365}	$0.55^{0.04}_{0.03}$
55072	31	6818^{481}_{414}	$0.55^{0.04}_{0.04}$
55073	32	6640^{357}_{308}	$0.54^{0.04}_{0.03}$
55074	33	6660^{377}_{335}	$0.53^{0.03}_{0.02}$
55075	34	6640^{381}_{330}	$0.54^{0.03}_{0.03}$
55077	36	6380^{346}_{303}	$0.51^{0.03}_{0.02}$
55079	38	6340^{332}_{310}	$0.51^{0.03}_{0.02}$
55082	41	6260^{319}_{303}	$0.51^{0.02}_{0.02}$
55083	42	6120^{312}_{284}	$0.50^{0.02}_{0.02}$
55084	43	6139^{341}_{301}	$0.50^{0.02}_{0.02}$
55085	44	6130^{322}_{278}	$0.50^{0.03}_{0.02}$
55086	45	6140^{304}_{290}	$0.50^{0.02}_{0.02}$
55087	46	6140^{321}_{284}	$0.51^{0.02}_{0.02}$
55088	47	6100^{302}_{273}	$0.50^{0.02}_{0.02}$
55089	48	5940^{239}_{221}	$0.49^{0.02}_{0.02}$
55090	49	5950^{290}_{274}	$0.49^{0.02}_{0.02}$
55091	50	5900^{290}_{265}	$0.49^{0.02}_{0.02}$
55092	51	5870^{301}_{270}	$0.49^{0.02}_{0.02}$
55093	52	5880^{289}_{262}	$0.49^{0.02}_{0.02}$
55094	53	5880^{282}_{251}	$0.49^{0.02}_{0.02}$
55095	54	5745^{514}_{318}	$0.48^{0.02}_{0.02}$
55096	55	5960^{318}_{273}	$0.49^{0.02}_{0.01}$
55097	56	5940^{307}_{278}	$0.49^{0.02}_{0.01}$
55099	58	5840^{300}_{265}	$0.48^{0.02}_{0.02}$
55100	59	5870^{322}_{294}	$0.48^{0.02}_{0.01}$
55104	63	5840^{305}_{286}	$0.49^{0.02}_{0.01}$
55105	64	5820^{316}_{272}	$0.49^{0.02}_{0.01}$
55109	68	5760^{304}_{271}	$0.48^{0.02}_{0.01}$
55111	70	5720^{308}_{259}	$0.48^{0.02}_{0.01}$
55116	75	5360^{203}_{191}	$0.47^{0.02}_{0.01}$
55117	76	5520^{251}_{237}	$0.48^{0.02}_{0.01}$
55121	80	5540^{250}_{234}	$0.48^{0.02}_{0.01}$
55122	81	5520^{234}_{230}	$0.48^{0.01}_{0.01}$
55124	83	5500^{244}_{218}	$0.48^{0.01}_{0.01}$
55128	87	5260^{146}_{154}	$0.48^{0.01}_{0.01}$
55131	90	5500^{232}_{227}	$0.48^{0.01}_{0.01}$
55132	91	5480^{244}_{214}	$0.48^{0.01}_{0.01}$
55134	93	5480^{241}_{216}	$0.48^{0.01}_{0.01}$

Table A1 – *continued* A List of the Temperatures and Bolometric Luminosities

55137	96	5480^{237}_{219}	$0.48^{0.01}_{0.01}$
55138	97	5460^{239}_{214}	$0.48^{0.01}_{0.01}$
55141	100	5520^{259}_{230}	$0.48^{0.01}_{0.01}$
55146	105	5460^{242}_{209}	$0.47^{0.01}_{0.01}$
55147	106	5460^{237}_{213}	$0.47^{0.01}_{0.01}$
SN2012A			
55937	8	15960^{636}_{594}	$1.62^{0.12}_{0.11}$
55938	9	13700^{1166}_{641}	$1.43^{0.21}_{0.14}$
55939	10	12039^{567}_{503}	$1.17^{0.08}_{0.07}$
55940	11	11043^{464}_{961}	$1.06^{0.09}_{0.15}$
55941	12	10837^{710}_{600}	$1.04^{0.16}_{0.11}$
55942	13	10665^{482}_{432}	$1.04^{0.08}_{0.06}$
55943	14	10459^{535}_{441}	$1.02^{0.08}_{0.06}$
55945	16	10106^{473}_{428}	$0.98^{0.07}_{0.06}$
55948	19	9034^{709}_{653}	$0.82^{0.10}_{0.07}$
55949	20	9020^{671}_{572}	$0.82^{0.09}_{0.07}$
55951	22	8680^{787}_{661}	$0.79^{0.10}_{0.07}$
55952	23	8577^{803}_{633}	$0.78^{0.11}_{0.07}$
55953	24	8261^{1105}_{622}	$0.73^{0.17}_{0.07}$
55954	25	7960^{490}_{416}	$0.70^{0.05}_{0.04}$
55955	26	7800^{492}_{416}	$0.68^{0.05}_{0.04}$
55957	28	7620^{403}_{384}	$0.64^{0.04}_{0.03}$
55958	29	7519^{484}_{398}	$0.63^{0.05}_{0.03}$
55962	33	7540^{453}_{408}	$0.63^{0.05}_{0.04}$
55966	37	7099^{670}_{450}	$0.58^{0.07}_{0.04}$
55967	38	7194^{552}_{519}	$0.59^{0.05}_{0.05}$
55969	40	7179^{606}_{365}	$0.58^{0.05}_{0.03}$
55972	43	7320^{538}_{453}	$0.58^{0.05}_{0.04}$
55974	45	7320^{571}_{472}	$0.58^{0.05}_{0.04}$
55975	46	7235^{592}_{442}	$0.58^{0.05}_{0.04}$
55976	47	7220^{509}_{436}	$0.57^{0.05}_{0.04}$
55977	48	7160^{504}_{422}	$0.57^{0.04}_{0.03}$
55979	50	6959^{488}_{404}	$0.54^{0.04}_{0.03}$
55981	52	6940^{503}_{408}	$0.53^{0.04}_{0.03}$
55982	53	6940^{509}_{437}	$0.52^{0.04}_{0.03}$
55983	54	6840^{483}_{404}	$0.52^{0.04}_{0.03}$
55984	55	6840^{468}_{419}	$0.52^{0.04}_{0.03}$
55985	56	6940^{491}_{413}	$0.52^{0.04}_{0.03}$
55987	58	6680^{467}_{404}	$0.49^{0.04}_{0.03}$
55988	59	6420^{414}_{363}	$0.47^{0.03}_{0.02}$
55991	62	6520^{441}_{391}	$0.48^{0.03}_{0.03}$
55992	63	6680^{401}_{354}	$0.49^{0.03}_{0.02}$
55993	64	6760^{391}_{355}	$0.50^{0.03}_{0.03}$
55994	65	6820^{392}_{365}	$0.50^{0.03}_{0.03}$

Table A1 – *continued* A List of the Temperatures and Bolometric Luminosities

55999	70	6653^{419}_{350}	$0.46^{0.03}_{0.03}$
56000	71	6580^{361}_{320}	$0.46^{0.02}_{0.02}$
56001	72	6665^{361}_{328}	$0.45^{0.03}_{0.02}$
56002	73	6657^{431}_{340}	$0.43^{0.03}_{0.02}$
56003	74	6600^{328}_{289}	$0.43^{0.02}_{0.02}$
56004	75	6600^{329}_{306}	$0.43^{0.02}_{0.02}$
56005	76	6620^{323}_{291}	$0.42^{0.02}_{0.02}$
56006	77	6600^{280}_{266}	$0.42^{0.02}_{0.02}$
56008	79	6600^{294}_{270}	$0.41^{0.02}_{0.02}$
56009	80	6590^{306}_{279}	$0.40^{0.02}_{0.02}$
56010	81	6680^{322}_{283}	$0.40^{0.02}_{0.02}$
56011	82	6700^{345}_{303}	$0.39^{0.02}_{0.02}$
56012	83	6560^{236}_{204}	$0.38^{0.02}_{0.01}$
56014	85	6600^{249}_{220}	$0.37^{0.04}_{0.03}$
56015	86	6640^{235}_{234}	$0.36^{0.02}_{0.01}$
56016	87	6600^{232}_{215}	$0.35^{0.02}_{0.02}$
56017	88	6587^{242}_{220}	$0.34^{0.02}_{0.02}$
56019	90	6600^{236}_{203}	$0.33^{0.02}_{0.01}$
56021	92	6600^{234}_{218}	$0.32^{0.01}_{0.01}$
56023	94	6700^{211}_{195}	$0.30^{0.01}_{0.01}$
56027	98	6725^{339}_{283}	$0.28^{0.02}_{0.02}$
56030	101	6600^{271}_{265}	$0.24^{0.01}_{0.02}$
56031	102	6400^{238}_{225}	$0.22^{0.01}_{0.01}$
56033	104	6280^{252}_{237}	$0.20^{0.01}_{0.01}$
56034	105	6240^{197}_{184}	$0.19^{0.01}_{0.01}$
56035	106	6200^{232}_{214}	$0.18^{0.01}_{0.01}$
56037	108	6100^{216}_{209}	$0.16^{0.01}_{0.01}$
56039	110	5540^{212}_{186}	$0.12^{0.01}_{0.01}$
SN2012aw			
56006	4	14235^{1153}_{675}	$2.60^{0.28}_{0.17}$
56007	5	13752^{556}_{508}	$2.53^{0.15}_{0.13}$
56008	6	12549^{607}_{527}	$2.34^{0.14}_{0.11}$
56009	7	11889^{491}_{481}	$2.25^{0.12}_{0.09}$
56010	8	11479^{423}_{371}	$2.22^{0.09}_{0.08}$
56011	9	11239^{571}_{567}	$2.20^{0.17}_{0.14}$
56012	10	10805^{329}_{309}	$2.09^{0.09}_{0.08}$
56013	11	10639^{320}_{298}	$2.04^{0.08}_{0.07}$
56014	12	10214^{333}_{296}	$1.97^{0.08}_{0.07}$
56015	13	9760^{219}_{205}	$1.85^{0.05}_{0.04}$
56016	14	9553^{320}_{398}	$1.80^{0.07}_{0.09}$
56017	15	9139^{288}_{262}	$1.70^{0.06}_{0.05}$
56018	16	8930^{251}_{203}	$1.67^{0.04}_{0.04}$
56019	17	8454^{379}_{464}	$1.60^{0.05}_{0.07}$
56020	18	7980^{137}_{126}	$1.55^{0.05}_{0.04}$

Table A1 – *continued* A List of the Temperatures and Bolometric Luminosities

56022	20	7640^{124}_{111}	$1.49^{0.04}_{0.04}$
56024	22	7400^{127}_{124}	$1.46^{0.04}_{0.04}$
56025	23	7377^{182}_{226}	$1.46^{0.06}_{0.06}$
56026	24	7260^{159}_{165}	$1.43^{0.06}_{0.05}$
56027	25	7160^{160}_{150}	$1.40^{0.06}_{0.05}$
56028	26	7120^{148}_{156}	$1.40^{0.06}_{0.05}$
56029	27	7020^{162}_{144}	$1.37^{0.05}_{0.05}$
56030	28	6965^{177}_{180}	$1.36^{0.05}_{0.05}$
56031	29	6880^{146}_{148}	$1.34^{0.05}_{0.05}$
56032	30	6792^{184}_{147}	$1.33^{0.05}_{0.05}$
56033	31	6740^{136}_{141}	$1.32^{0.04}_{0.04}$
56034	32	6700^{134}_{136}	$1.31^{0.04}_{0.04}$
56035	33	6628^{176}_{143}	$1.30^{0.05}_{0.04}$
56036	34	6621^{210}_{229}	$1.28^{0.05}_{0.05}$
56037	35	6540^{207}_{208}	$1.27^{0.05}_{0.04}$
56039	37	6440^{204}_{197}	$1.26^{0.05}_{0.04}$
56040	38	6425^{212}_{196}	$1.27^{0.05}_{0.05}$
56041	39	6438^{264}_{225}	$1.27^{0.05}_{0.05}$
56042	40	6440^{218}_{189}	$1.28^{0.06}_{0.04}$
56043	41	6380^{178}_{176}	$1.28^{0.05}_{0.05}$
56044	42	6360^{179}_{173}	$1.28^{0.05}_{0.05}$
56046	44	6280^{177}_{166}	$1.27^{0.05}_{0.05}$
56047	45	6233^{183}_{172}	$1.26^{0.05}_{0.04}$
56049	47	6160^{168}_{159}	$1.25^{0.05}_{0.05}$
56050	48	6100^{128}_{138}	$1.26^{0.05}_{0.04}$
56051	49	6000^{160}_{153}	$1.25^{0.05}_{0.04}$
56052	50	5813^{165}_{147}	$1.24^{0.04}_{0.04}$
56053	51	5780^{154}_{141}	$1.24^{0.04}_{0.04}$
56054	52	6080^{209}_{209}	$1.27^{0.04}_{0.04}$
56056	54	6140^{227}_{200}	$1.27^{0.04}_{0.04}$
56057	55	6209^{263}_{238}	$1.29^{0.04}_{0.04}$
56058	56	6280^{243}_{211}	$1.30^{0.04}_{0.04}$
56059	57	6380^{253}_{222}	$1.31^{0.04}_{0.03}$
56061	59	6420^{258}_{218}	$1.32^{0.04}_{0.03}$
56062	60	6375^{249}_{238}	$1.31^{0.04}_{0.05}$
56064	62	6420^{242}_{227}	$1.32^{0.05}_{0.04}$
56066	64	6060^{166}_{161}	$1.29^{0.05}_{0.04}$
56070	68	6000^{144}_{146}	$1.28^{0.05}_{0.04}$
56072	70	5960^{164}_{152}	$1.26^{0.05}_{0.04}$
56086	84	5900^{151}_{158}	$1.23^{0.05}_{0.05}$
56087	85	5840^{154}_{140}	$1.21^{0.05}_{0.05}$
56088	86	5480^{172}_{152}	$1.11^{0.06}_{0.05}$
56089	87	5480^{156}_{139}	$1.11^{0.05}_{0.05}$
56097	95	5760^{123}_{107}	$1.13^{0.05}_{0.05}$

Table A1 – *continued* A List of the Temperatures and Bolometric Luminosities

SN2012ec			
56154	11	10020^{345}_{326}	$2.26^{0.09}_{0.08}$
56155	12	9780^{332}_{304}	$2.14^{0.08}_{0.07}$
56158	15	9068^{926}_{534}	$1.85^{0.16}_{0.13}$
56159	16	8080^{203}_{196}	$1.69^{0.04}_{0.04}$
56165	22	6880^{101}_{107}	$1.44^{0.15}_{0.13}$
56168	25	6640^{101}_{88}	$1.36^{0.14}_{0.12}$
56171	28	6480^{92}_{100}	$1.33^{0.13}_{0.10}$
56173	30	6620^{148}_{134}	$1.40^{0.29}_{0.19}$
56176	33	6560^{136}_{142}	$1.40^{0.17}_{0.12}$
56179	36	6200^{124}_{132}	$1.28^{0.11}_{0.09}$
56181	38	6160^{115}_{122}	$1.27^{0.15}_{0.12}$
56182	39	6120^{110}_{123}	$1.26^{0.06}_{0.05}$
56186	43	6180^{125}_{129}	$1.30^{0.05}_{0.04}$
56190	47	6120^{127}_{108}	$1.28^{0.05}_{0.05}$
56195	52	6150^{152}_{136}	$1.32^{0.06}_{0.06}$
56199	56	6220^{127}_{116}	$1.36^{0.04}_{0.04}$
56202	59	6099^{159}_{151}	$1.32^{0.04}_{0.05}$
56204	61	6000^{122}_{103}	$1.29^{0.04}_{0.04}$
56208	65	5960^{133}_{122}	$1.30^{0.04}_{0.03}$
56211	68	5840^{106}_{104}	$1.25^{0.04}_{0.03}$
56212	69	5780^{107}_{122}	$1.24^{0.04}_{0.04}$
56216	73	5680^{113}_{104}	$1.22^{0.05}_{0.05}$
SN2013ab			
56344	4	17620^{330}_{299}	$5.54^{0.18}_{0.16}$
56345	5	15490^{596}_{534}	$4.73^{0.35}_{0.25}$
56346	6	14258^{1073}_{911}	$4.15^{0.40}_{0.32}$
56347	7	12768^{570}_{491}	$3.66^{0.19}_{0.16}$
56348	8	11885^{268}_{254}	$3.35^{0.11}_{0.10}$
56349	9	11210^{326}_{401}	$3.07^{0.13}_{0.15}$
56350	10	10380^{105}_{112}	$2.73^{0.04}_{0.04}$
56351	11	9996^{231}_{387}	$2.54^{0.09}_{0.12}$
56352	12	9645^{264}_{266}	$2.41^{0.08}_{0.08}$
56353	13	9349^{250}_{233}	$2.21^{0.10}_{0.09}$
56354	14	9040^{183}_{160}	$2.09^{0.04}_{0.04}$
56355	15	8928^{465}_{257}	$2.04^{0.13}_{0.06}$
56356	16	9080^{282}_{284}	$2.04^{0.07}_{0.07}$
56357	17	8826^{390}_{329}	$2.00^{0.09}_{0.07}$
56358	18	8690^{267}_{257}	$1.96^{0.06}_{0.06}$
56359	19	8620^{268}_{243}	$1.94^{0.06}_{0.05}$
56360	20	8368^{315}_{286}	$1.87^{0.07}_{0.06}$
56361	21	8220^{233}_{226}	$1.83^{0.05}_{0.04}$
56362	22	7960^{229}_{201}	$1.75^{0.04}_{0.04}$

Table A1 – *continued* A List of the Temperatures and Bolometric Luminosities

56363	23	7920^{223}_{202}	$1.74^{0.04}_{0.04}$
56364	24	7560^{202}_{182}	$1.67^{0.04}_{0.03}$
56365	25	7540^{195}_{186}	$1.65^{0.03}_{0.03}$
56366	26	7380^{215}_{198}	$1.57^{0.04}_{0.04}$
56368	28	7190^{560}_{206}	$1.51^{0.10}_{0.04}$
56370	30	7080^{354}_{335}	$1.44^{0.06}_{0.05}$
56372	32	7016^{452}_{380}	$1.40^{0.08}_{0.05}$
56373	33	6940^{349}_{309}	$1.37^{0.05}_{0.04}$
56374	34	6800^{329}_{303}	$1.34^{0.05}_{0.04}$
56376	36	6720^{327}_{290}	$1.31^{0.04}_{0.04}$
56377	37	6680^{314}_{293}	$1.29^{0.04}_{0.04}$
56378	38	6680^{333}_{309}	$1.28^{0.04}_{0.04}$
56380	40	6620^{315}_{282}	$1.26^{0.04}_{0.03}$
56381	41	6580^{315}_{275}	$1.25^{0.04}_{0.03}$
56382	42	6500^{290}_{281}	$1.24^{0.04}_{0.03}$
56383	43	6580^{313}_{276}	$1.22^{0.04}_{0.03}$
56384	44	6650^{329}_{294}	$1.23^{0.04}_{0.03}$
56388	48	6260^{278}_{255}	$1.19^{0.03}_{0.03}$
56389	49	6220^{283}_{274}	$1.17^{0.03}_{0.03}$
56390	50	6240^{293}_{267}	$1.15^{0.03}_{0.03}$
56394	54	6299^{408}_{325}	$1.14^{0.05}_{0.03}$
56395	55	6380^{319}_{271}	$1.15^{0.04}_{0.03}$
56397	57	6500^{313}_{299}	$1.15^{0.04}_{0.03}$
56398	58	6380^{303}_{284}	$1.13^{0.03}_{0.03}$
56402	62	6300^{306}_{267}	$1.13^{0.03}_{0.03}$
56403	63	6280^{307}_{264}	$1.10^{0.03}_{0.03}$
56404	64	6380^{308}_{280}	$1.14^{0.03}_{0.03}$
56405	65	6320^{292}_{283}	$1.13^{0.03}_{0.03}$
56406	66	6240^{308}_{288}	$1.12^{0.03}_{0.03}$
56407	67	6220^{293}_{264}	$1.11^{0.03}_{0.02}$
56409	69	6347^{378}_{311}	$1.14^{0.04}_{0.03}$
56411	71	6300^{293}_{278}	$1.13^{0.03}_{0.03}$
56412	72	6220^{297}_{261}	$1.10^{0.03}_{0.03}$
56413	73	6180^{302}_{251}	$1.07^{0.03}_{0.02}$
56414	74	6120^{262}_{246}	$1.06^{0.02}_{0.02}$
56415	75	6700^{381}_{344}	$1.13^{0.05}_{0.04}$
56416	76	6460^{362}_{309}	$1.09^{0.04}_{0.03}$
56419	79	6140^{286}_{252}	$1.05^{0.03}_{0.02}$
56420	80	6080^{264}_{260}	$1.05^{0.02}_{0.02}$
56421	81	5760^{244}_{224}	$1.01^{0.02}_{0.02}$
56422	82	5960^{259}_{244}	$1.02^{0.02}_{0.02}$
56423	83	5940^{264}_{237}	$1.01^{0.02}_{0.02}$
56426	86	6115^{411}_{354}	$0.99^{0.04}_{0.03}$
56427	87	5800^{251}_{236}	$0.95^{0.02}_{0.02}$
56428	88	5760^{256}_{217}	$0.94^{0.02}_{0.02}$

Table A1 – *continued* A List of the Temperatures and Bolometric Luminosities

56429	89	6020^{272}_{247}	$0.95^{0.02}_{0.02}$
56430	90	5860^{255}_{223}	$0.92^{0.02}_{0.02}$
56431	91	5760^{246}_{215}	$0.90^{0.02}_{0.02}$
56432	92	6180^{330}_{280}	$0.90^{0.03}_{0.02}$
56433	93	5776^{646}_{393}	$0.86^{0.06}_{0.03}$
56434	94	5580^{229}_{207}	$0.83^{0.02}_{0.02}$
56435	95	5663^{444}_{302}	$0.82^{0.02}_{0.02}$
56436	96	5900^{299}_{254}	$0.81^{0.02}_{0.02}$
56437	97	5780^{277}_{250}	$0.75^{0.02}_{0.02}$
56438	98	5664^{365}_{317}	$0.69^{0.03}_{0.03}$
56439	99	5760^{276}_{247}	$0.66^{0.01}_{0.01}$
56440	100	5446^{318}_{287}	$0.62^{0.02}_{0.02}$
56441	101	5480^{245}_{224}	$0.59^{0.01}_{0.01}$
56442	102	5112^{460}_{477}	$0.54^{0.02}_{0.02}$
56443	103	4860^{247}_{222}	$0.49^{0.02}_{0.02}$
56444	104	4865^{470}_{353}	$0.46^{0.02}_{0.02}$
56445	105	4840^{236}_{227}	$0.42^{0.02}_{0.02}$
56446	106	4700^{233}_{204}	$0.40^{0.02}_{0.02}$
56448	108	4380^{159}_{137}	$0.37^{0.01}_{0.01}$
56449	109	4580^{176}_{148}	$0.35^{0.01}_{0.01}$
56451	111	4500^{170}_{143}	$0.31^{0.01}_{0.01}$
56454	114	4880^{237}_{234}	$0.27^{0.01}_{0.01}$
56456	116	4620^{226}_{196}	$0.28^{0.01}_{0.01}$
56457	117	4840^{180}_{181}	$0.27^{0.01}_{0.01}$
56458	118	4880^{194}_{174}	$0.26^{0.01}_{0.01}$
56460	120	4760^{173}_{176}	$0.25^{0.01}_{0.01}$
56461	121	5520^{343}_{295}	$0.25^{0.01}_{0.01}$
56464	124	4808^{243}_{208}	$0.24^{0.01}_{0.01}$
56466	126	4770^{202}_{186}	$0.24^{0.01}_{0.01}$
56468	128	4460^{209}_{193}	$0.26^{0.02}_{0.01}$
56470	130	4620^{235}_{199}	$0.24^{0.01}_{0.01}$
56476	136	4480^{220}_{187}	$0.24^{0.01}_{0.01}$
56477	137	4800^{242}_{225}	$0.23^{0.01}_{0.01}$
56478	138	4980^{256}_{248}	$0.21^{0.01}_{0.01}$
56479	139	4680^{241}_{205}	$0.22^{0.01}_{0.01}$
56480	140	4800^{242}_{225}	$0.21^{0.01}_{0.01}$
56481	141	4640^{225}_{211}	$0.22^{0.01}_{0.01}$
56485	145	5080^{278}_{248}	$0.20^{0.01}_{0.01}$
56487	147	4940^{255}_{241}	$0.20^{0.01}_{0.01}$
56489	149	4840^{287}_{250}	$0.19^{0.01}_{0.01}$
SN2013by			
56407	0	22890^{833}_{781}	$23.65^{1.80}_{1.62}$
56408	1	19258^{1096}_{704}	$18.89^{2.62}_{1.74}$
56409	2	16860^{549}_{512}	$16.23^{0.99}_{0.88}$

Table A1 – *continued* A List of the Temperatures and Bolometric Luminosities

56410	3	14923^{704}_{552}	$13.53^{1.09}_{0.79}$
56411	4	13940^{350}_{343}	$12.41^{0.51}_{0.48}$
56412	5	12422^{491}_{1173}	$10.76^{0.65}_{1.36}$
56413	6	11304^{440}_{389}	$9.73^{0.51}_{0.43}$
56414	7	10875^{562}_{477}	$9.09^{0.70}_{0.48}$
56416	9	9991^{474}_{437}	$8.12^{0.34}_{0.32}$
56417	10	9500^{289}_{275}	$7.47^{0.24}_{0.22}$
56418	11	9340^{287}_{253}	$7.29^{0.23}_{0.19}$
56419	12	8984^{487}_{309}	$6.88^{0.21}_{0.26}$
56423	16	8272^{581}_{334}	$5.54^{0.35}_{0.19}$
56424	17	8377^{379}_{359}	$5.36^{0.27}_{0.30}$
56426	19	8060^{324}_{305}	$4.88^{0.16}_{0.14}$
56427	20	7794^{736}_{607}	$4.58^{0.43}_{0.32}$
56428	21	8455^{881}_{724}	$4.91^{0.63}_{0.43}$
56429	22	8540^{895}_{743}	$4.89^{0.64}_{0.45}$
56434	27	7180^{601}_{513}	$3.65^{0.25}_{0.18}$
56436	29	7010^{587}_{486}	$3.48^{0.23}_{0.16}$
56437	30	6880^{563}_{455}	$3.38^{0.20}_{0.14}$
56438	31	7020^{574}_{485}	$3.38^{0.21}_{0.15}$
56439	32	6720^{518}_{450}	$3.18^{0.16}_{0.12}$
56440	33	6700^{520}_{436}	$3.18^{0.16}_{0.12}$
56442	35	6620^{511}_{422}	$3.14^{0.15}_{0.11}$
56444	37	6576^{493}_{430}	$3.12^{0.14}_{0.11}$
56445	38	6640^{509}_{432}	$2.89^{0.14}_{0.10}$
56447	40	6478^{602}_{518}	$2.88^{0.13}_{0.12}$
56448	41	6720^{509}_{450}	$2.92^{0.15}_{0.11}$
56449	42	6305^{807}_{635}	$2.79^{0.20}_{0.14}$
56450	43	6180^{442}_{363}	$2.78^{0.09}_{0.08}$
56451	44	6520^{484}_{417}	$2.81^{0.12}_{0.09}$
56453	46	5900^{382}_{342}	$2.50^{0.07}_{0.07}$
56456	49	5860^{384}_{332}	$2.50^{0.07}_{0.07}$
56458	51	5760^{367}_{321}	$2.42^{0.07}_{0.06}$
56460	53	5660^{363}_{302}	$2.35^{0.07}_{0.06}$
56462	55	5720^{368}_{311}	$2.29^{0.06}_{0.06}$
56464	57	5780^{375}_{321}	$2.23^{0.06}_{0.06}$
56465	58	5620^{337}_{315}	$2.18^{0.06}_{0.06}$
56466	59	5480^{324}_{294}	$2.15^{0.07}_{0.06}$
56468	61	5820^{376}_{330}	$2.08^{0.06}_{0.06}$
56470	63	5880^{377}_{341}	$2.03^{0.06}_{0.05}$
56472	65	5620^{351}_{304}	$1.95^{0.06}_{0.05}$
56473	66	5640^{348}_{309}	$1.89^{0.06}_{0.05}$
56474	67	5660^{353}_{311}	$1.81^{0.05}_{0.05}$
56476	69	5400^{319}_{281}	$1.70^{0.06}_{0.05}$
56477	70	5420^{330}_{277}	$1.58^{0.05}_{0.05}$
56478	71	5380^{315}_{280}	$1.54^{0.05}_{0.05}$

Table A1 – *continued* A List of the Temperatures and Bolometric Luminosities

56481	74	5183^{296}_{278}	$1.40^{0.06}_{0.07}$
56482	75	5173^{286}_{261}	$1.34^{0.05}_{0.05}$
56483	76	5188^{294}_{258}	$1.26^{0.05}_{0.04}$
56486	79	5080^{270}_{255}	$1.07^{0.05}_{0.04}$
56487	80	5012^{282}_{263}	$1.00^{0.05}_{0.05}$
56488	81	4816^{255}_{234}	$0.88^{0.05}_{0.04}$
56489	82	5172^{391}_{433}	$0.76^{0.05}_{0.10}$
SN2013ej			
56500	3	13900^{724}_{841}	$4.00^{0.33}_{0.28}$
56501	4	13053^{537}_{488}	$4.02^{0.29}_{0.24}$
56502	5	12853^{749}_{665}	$4.33^{0.46}_{0.38}$
56503	6	11493^{1170}_{173}	$4.14^{0.57}_{0.42}$
56504	7	11488^{757}_{559}	$4.19^{0.40}_{0.34}$
56505	8	11271^{646}_{407}	$4.08^{0.60}_{0.37}$
56506	9	11145^{625}_{625}	$4.28^{0.36}_{0.29}$
56507	10	10489^{534}_{450}	$4.07^{0.32}_{0.24}$
56508	11	10452^{545}_{539}	$4.07^{0.31}_{0.26}$
56509	12	10220^{480}_{433}	$4.02^{0.28}_{0.23}$
56510	13	10018^{1224}_{666}	$3.92^{0.86}_{0.35}$
56511	14	10600^{1302}_{995}	$4.41^{0.99}_{0.64}$
56512	15	10560^{1288}_{996}	$4.43^{0.98}_{0.64}$
56513	16	10339^{1448}_{1121}	$4.25^{1.16}_{0.74}$
56514	17	10183^{1525}_{972}	$4.20^{1.12}_{0.59}$
56515	18	9856^{1277}_{1043}	$3.91^{0.88}_{0.57}$
56516	19	9410^{848}_{709}	$3.67^{0.51}_{0.38}$
56520	23	9580^{1516}_{1108}	$3.83^{1.05}_{0.62}$
56521	24	9784^{1536}_{1125}	$3.95^{1.13}_{0.69}$
56522	25	9775^{1558}_{1142}	$3.84^{1.11}_{0.65}$
56524	27	8975^{1547}_{979}	$3.22^{0.93}_{0.46}$
56525	28	9054^{1368}_{1187}	$3.29^{0.82}_{0.56}$
56526	29	8620^{1138}_{855}	$3.03^{0.61}_{0.38}$
56528	31	8640^{1144}_{860}	$2.93^{0.59}_{0.37}$
56529	32	8737^{1154}_{896}	$2.93^{0.60}_{0.40}$
56533	36	8180^{1006}_{791}	$2.50^{0.43}_{0.28}$
56534	37	8060^{1004}_{781}	$2.42^{0.41}_{0.26}$
56538	41	7040^{1359}_{962}	$1.91^{0.43}_{0.21}$
56539	42	7560^{1394}_{1000}	$2.02^{0.51}_{0.27}$
56541	44	7520^{1363}_{997}	$1.92^{0.47}_{0.25}$
56544	47	7400^{1301}_{971}	$1.84^{0.42}_{0.23}$
56546	49	6920^{1157}_{840}	$1.65^{0.31}_{0.16}$
56553	56	6520^{968}_{757}	$1.48^{0.21}_{0.12}$
56554	57	6940^{1124}_{853}	$1.53^{0.28}_{0.16}$
56560	63	6580^{1023}_{751}	$1.35^{0.21}_{0.11}$
56562	65	6520^{968}_{757}	$1.35^{0.19}_{0.11}$

Table A1 – *continued* A List of the Temperatures and Bolometric Luminosities

56563	66	6800^{1097}_{805}	$1.34^{0.24}_{0.12}$
56567	70	6440^{953}_{732}	$1.25^{0.17}_{0.09}$
56568	71	6340^{915}_{713}	$1.21^{0.16}_{0.09}$
56573	76	6600^{1003}_{771}	$1.16^{0.18}_{0.10}$
56574	77	6800^{1097}_{805}	$1.16^{0.21}_{0.11}$
56577	80	6920^{1125}_{843}	$1.14^{0.21}_{0.11}$
56578	81	6540^{981}_{758}	$1.05^{0.15}_{0.09}$
56589	92	6700^{1056}_{784}	$0.79^{0.13}_{0.07}$
56594	97	6560^{993}_{759}	$0.59^{0.09}_{0.05}$
56596	99	5980^{812}_{630}	$0.44^{0.04}_{0.02}$
56600	103	6420^{1135}_{837}	$0.22^{0.04}_{0.02}$
56607	110	6180^{1358}_{933}	$0.15^{0.03}_{0.01}$
56610	113	6980^{2924}_{1539}	$0.16^{0.09}_{0.02}$
56613	116	5960^{1815}_{1111}	$0.12^{0.03}_{0.01}$
56616	119	6440^{1638}_{1072}	$0.13^{0.03}_{0.01}$
56617	120	5960^{1722}_{1075}	$0.13^{0.03}_{0.01}$